Table 2. Expression of transcription factors in B-lymphoma cells

	Blimp-1	CIIA	c-Rel	Oct-2	p50	p65	Pax5
Splenic B cell	–	+	+	+	+	+	+
B-lymphoma cell	–	+	–	–	+	+	+

The results of RT-PCR analysis for expression of transcription factors are shown. RT-PCR was performed using total RNA samples obtained from splenic B cells of wild-type mice or B-lymphoma cells generated from EGFP-transgenic mice according to the protocol in "Methods." The results are described as to whether PCR products are confirmed or not in electrophoresis (+ or –, respectively).

mice lost body weight and showed hematopoietic abnormalities, including marked leukocytosis and severe anemia, with ascites and massive splenomegaly (Figure 1B). Morphologic analyses revealed that atypical lymphocytes with coarse and pachychromatic nuclei were the prevalent population in the peripheral blood and spleen (Figure 1C). Few cells with these morphologic features were observed in the BM. When these cells were isolated from the peripheral blood, spleen, and lymph nodes, they expressed B220, CD5, and IgM, as well as EGFP (Figure 1D). Development of the same abnormal cell phenotype was observed in one-half of the progeny generated by mating the F1 mice (6 of 12 mice in the F2) and in a third of the progeny generated by mating the F2 mice (7 of 21 mice in the F3) with wild-type B6 mice, suggesting that some proviruses integrated and transmitted to the progeny were involved in leukemogenesis to B-cell lymphoma.

Characteristics of B-cell lymphoma

Because the emerging cells expressed B220 and IgM on their surfaces, we performed further analyses of markers and transcription factors characteristic of B lymphocyte differentiation. Expression of CD24, CD80, CD86, and MHC class II on B-lymphoma cells from EGFP-transgenic mice was similar to that on splenic B cells from wild-type B6 mice, whereas CD43 and CD5 expression was more prevalent in the B-lymphoma cells than in the wild-type splenic B cells (Table 1). Analysis of transcription factors, such as Pax5 and the NF-κB p50 and p65 components, also indicated that the lymphoma was derived from immature B cells (Table 2). Study of the immunoglobulin gene rearrangement pattern showed a monoclonal configuration (Figure 2A). Interestingly, although the cells proliferated vigorously in vitro (Figure 2B), they were prone to apoptosis, as shown by DNA fragmentation and propidium iodide staining. These changes were rescued by overexpression of the antiapoptotic Bcl-x_L molecule (Figure 2C-D). To assess the growth activity of the lymphoma cells in vivo, we transplanted them into NOD/SCID mice. When the NOD/SCID mice were intravenously inoculated with 1×10^5 cells, they showed aggressive leukocytosis and severe anemia with weight loss, massive splenomegaly, and ascites by 3 weeks after transplantation. Lymphoma cells obtained from spleen, lymph nodes, and BM of the NOD/SCID mice that underwent transplantation still

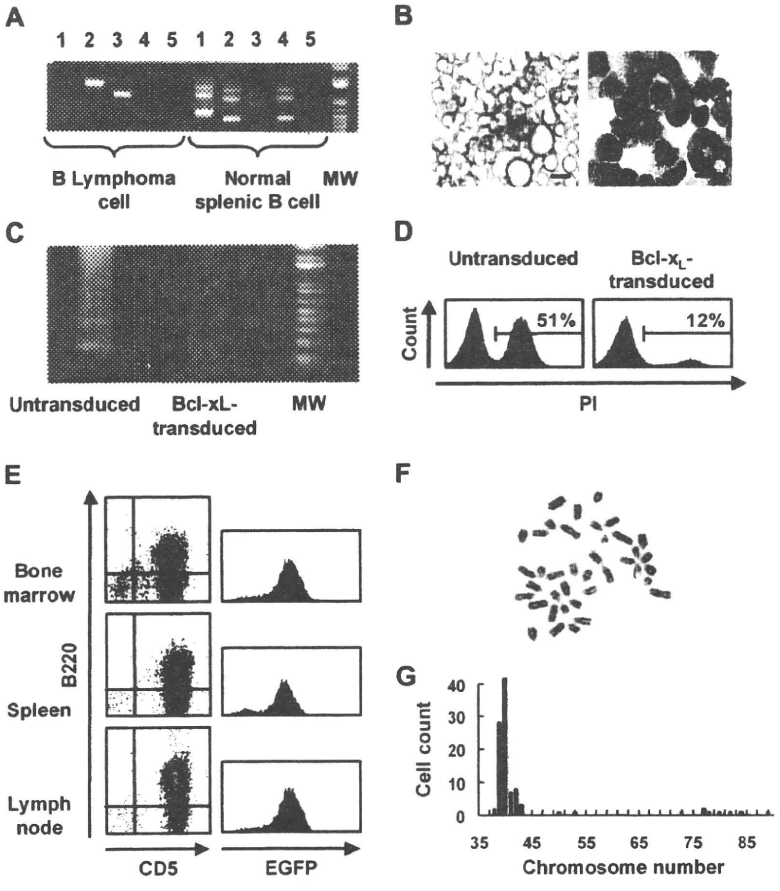

Figure 2. Characteristics of B-lymphoma cells generated from the transgenic mice. (A) PCR analysis of immunoglobulin gene rearrangement in splenic B cells of wild-type mice and B-lymphoma cells of transgenic mice. Lane 1 shows J558-J_H4; lane 2, 7183-J_H4; lane 3, Q52-J_H4; lane 4, D-J_H4; and lane 5, distilled water. (B) Morphologic appearance of B-lymphoma cells in vitro (left panel shows bright field in culture; right panel, May-Gruenwald-Giemsa staining of a cytospun sample; 63×/1.4 NA oil objective). Bars represent 10 μm. (C-D) Electrophoresis of genomic DNA (C) and propidium iodide staining (D) of untransduced or Bcl-x_L–transduced B-lymphoma cells. (E) Flow cytometric analysis of marrow, spleen, and lymph node cells in NOD/SCID mice that underwent transplantation with B-lymphoma cells at 4 weeks after transplantation. (F) Karyotype analysis of the B-lymphoma cells by Giemsa staining (100×/1.4 NA oil objective). (G) The number of chromosomes of B-lymphoma cells. MW indicates molecular weight marker in panels A and C.

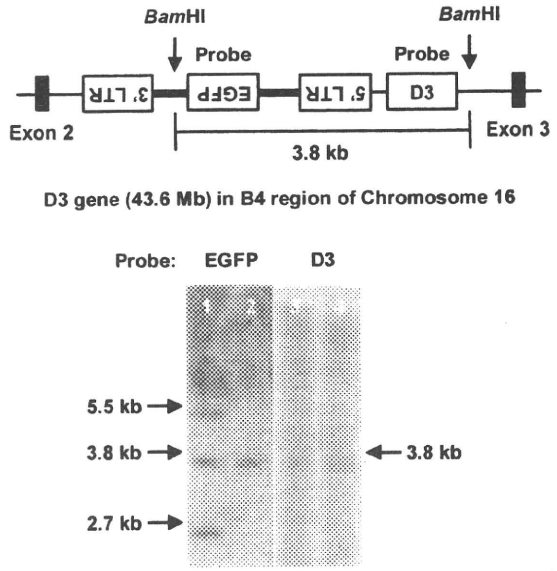

Figure 3. Identification of retroviral integration sites. (Top) A scheme of an integration site of the provirus into D3 locus determined on the basis of the results of LAM-PCR analysis. *Bam*HI sites and probes used in Southern blotting are also shown. (Bottom) Southern blotting of *Bam*HI-digested genomic DNA obtained from F1 (lanes 1 and 3) and F2 (lanes 2 and 4) of transgenic mice using an EGFP (lanes 1-2) or D3 (lanes 3-4) probe.

expressed B220, CD5, and EGFP, as observed before transplantation (Figure 2E). Because the karyotype analysis revealed that most of the cells were diploid (2n = 40), it was not likely that large chromosomal aberrations such as deletion, inversion, and translocation had caused the transformation events (Figure 2F-G). Lymphoma cells were able to establish disease in mice that received transplants after 12 passages in vivo, suggesting that their malignant potential was of a high grade.

Identification of the integration site relevant to the leukemogenesis

The number of provirus copies integrated into the chromosomes of the original chimeric mice decreased in their progeny, thus resulting in the generation of mice with a single provirus copy.[12] To identify an integration site relevant to the leukemogenesis, chimeric mice developing B-cell lymphoma were mated with B6 mice to obtain a single provirus progeny (Figure 3). The progeny mice developed the same hematologic signs, including leukocytosis, anemia, ascites, and splenomegaly, by the age of 1 year and were found to be affected by B-cell lymphoma with the identical phenotypes of surface antigens (EGFP, B220, and CD5) as the malignancy that developed in the original chimeric mice. To identify the integration site of the provirus, high-molecular-weight DNA was obtained and analyzed by LAM-PCR. BLAST analysis of the NCBI mouse DNA database resulted in identification of the provirus integration site between exons 2 and 3 of the *D3* gene in the reverse orientation (Figure 3 top panel). This result was also confirmed by Southern blot analysis in which the middle of 3 bands that hybridized with the EGFP probe also hybridized with the D3 probe in chimeric mice (lanes 1 and 3 in Figure 3 bottom panel). A single band hybridized with the EGFP probe in the F2 progeny was also hybridized with the D3 probe (lanes 2 and 4 in Figure 3 bottom panel, respectively).

As expected, the B-cell lymphoma cells expressed D3 at a higher level than normal splenic B cells (Figure 4A). The transcript size of the *D3* gene in the lymphoma cells was identical to that in the brain (Figure 4B), suggesting that there was no aberrance of the splicing mechanism. Quantitative RT-PCR revealed that the expression level was approximately 4 times that in normal B cells ($P < .05$; Figure 4C). Importantly, overexpression of the *D3* gene was observed only in B-cell lymphoma cells ($EGFP^+/CD5^+$; Figure 4D). Although $EGFP^+/CD5^-$ B cells also had the provirus integrated into the D3 locus, the level of D3 expression in these cells was significantly lower than that in the lymphoma cells and nearly as low as that in the splenic B cells of wild-type mice (Figure 4D), suggesting that integration of the provirus into the D3 locus was necessary, but not sufficient for leukemogenesis.

Involvement of D3 expression in B-cell differentiation

Mice with provirus integrations in the D3 locus selectively developed B-cell lymphoma, suggesting that overexpression of D3 could affect proliferation and/or differentiation of the B-cell lineage. D3, one of the members of the dopamine receptor family, which are G protein–coupled and 7-transmembrane receptors,

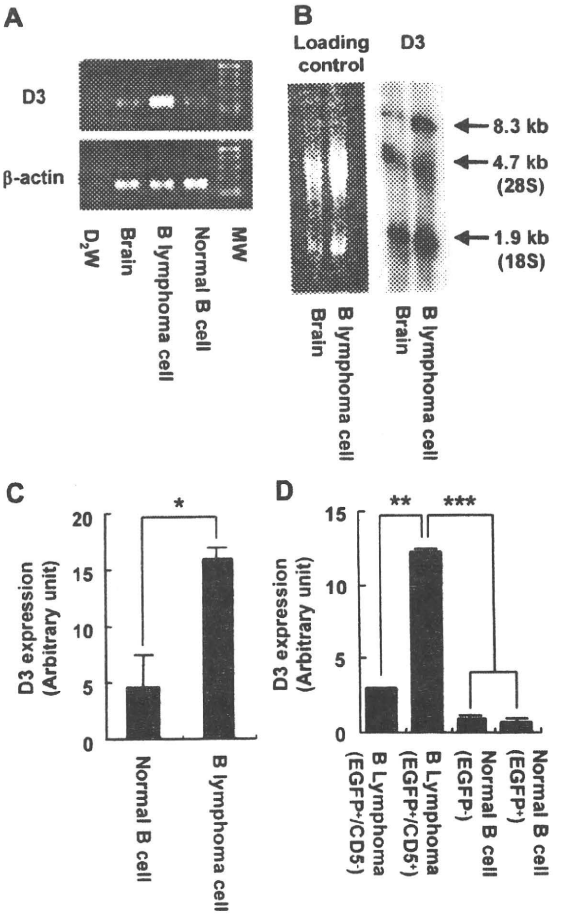

Figure 4. Activation of the *D3* gene in the transgenic mice. (A) RT-PCR analysis of D3 expression in brain and splenic B cells of wild-type mice, and B-lymphoma cells of transgenic mice. β-actin is used as an internal control. MW indicates molecular weight marker. (B) Northern blotting of total RNA obtained from brain or B-lymphoma cells using a D3 probe. Left panel is shown as a loading control. D3 transcripts are found at the size of 8.3 kb in the right panel. 28S and 18S indicate ribosomal RNA. (C) Quantitative RT-PCR analysis of D3 expression in normal splenic B cells and B-lymphoma cells. (D) Quantitative RT-PCR analysis of D3 expression in B-lymphoma cells ($CD5^-$ or $CD5^+$ in $EGFP^+$ population) and normal B cells ($EGFP^-$ or $EGFP^+$) in transgenic mice. Error bars are ± SD. $^*P < .05$; $^{**}P < .01$; $^{***}P < .005$ in panels C and D.

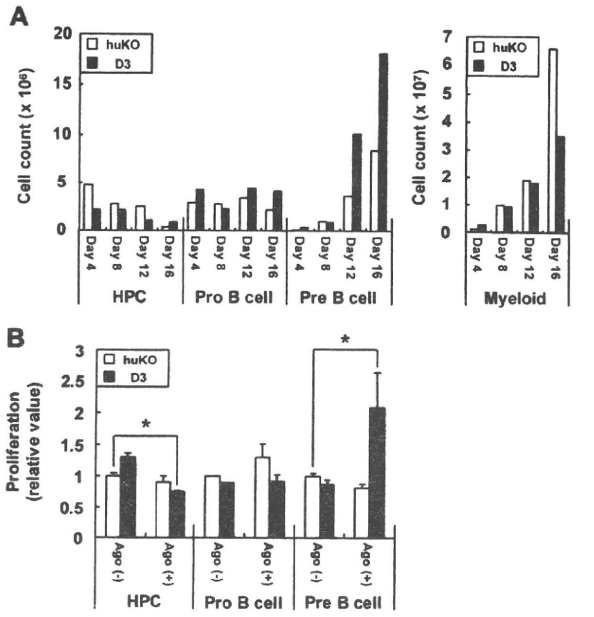

Figure 5. A role of D3 expression in B-cell development. (A) Coculture experiments of D3-transduced KL cells on PA6 cells in the presence of DPAT. The number of HPCs, pro-B, pre-B, and myeloid cells yielded from huKO- or D3-transduced KL cells (□ or ■, respectively) were shown. Representative data are shown in 2 independent experiments. (B) HPCs, pro-B, and pre-B cells derived from the transduced huKO-transduced (□) or D3-tranduced KL cells (■) cultured on PA6 cells were isolated and their proliferations were determined by the proliferation assay using [^{3}H]-thymidine in the presence or absence of DPAT (Ago + or −, respectively). Data are shown as normalized values to DPAT-free, huKO-transduced cultures in each cell population. Representative data are shown in 2 independent experiments. Error bars are ± SD. *$P < .05$.

inhibits neural activity by suppressing both the activity of the potassium ion channel and the production of cyclic adenosine monophosphate via inactivation of adenylate cyclase.[22] Although D3 is expressed in the brain (especially in the olfactory bulb), recent studies have reported that human peripheral blood lymphocytes such as naive CD8$^+$ T cells also express D3.[23] Simultaneously, a constant amount of dopamine is secreted and accumulated in the lymph nodes and plasma.[24-26] However, thus far there have been no reports of D3 expression in B cells and B-cell lymphoma. To assess the effect of D3 expression on the differentiation of hematopoietic progenitor cells (HPCs) into B cells, KL cells were transduced with the D3 cDNA by using the retroviral vector GCDsap and then cultured on the stromal cell line PA6 supplemented with IL-7 in the presence of the D3-specific agonist DPAT. D3-transduced cells proliferated and preferentially differentiated into pre-B cells over time; cells transduced with the huKO gene showed less proliferation and differentiation (Figure 5A). Importantly, D3-transduced pre-B cells in the presence of DPAT proliferated significantly ($P < .05$) more than huKO-transduced cells (Figure 5B). These results demonstrated that D3 signaling positively regulated not only the differentiation of HPCs into the B-cell lineage, but also the proliferation of pre-B cells.

Involvement of D3 expression in development of B-cell lymphoma

Having found that D3 expression preferentially induced the differentiation of HPCs into the B-cell lineage, we assessed whether D3-transduced cells transformed into B-cell lymphoma in vivo. Contrary to expectation, mice that received transplants of KL cells transduced with the *D3* gene showed neither preferential proliferation of B cells nor development of B-cell lymphoma (data not shown). Because the lymphoma observed in transgenic mice was highly sensitive to apoptosis, which was capable of rescue by the overexpression of the Bcl-x_L, KL cells were double-transduced with D3 and Bcl-x_L together with huKO and NGFR, respectively, and transplanted into lethally irradiated mice. Expression of both D3 and Bcl-x_L was confirmed by RT-PCR using peripheral blood cells obtained from mice 20 weeks after transplantation (Figure 6A). Whereas mice that underwent transplantation with D3-transduced or Bcl-x_L–transduced cells showed no abnormal hematopoiesis during a period of 40 weeks after transplantation, 3 mice represented as open symbols in Figure 6B, which had undergone transplantation with cells transduced with both D3 and Bcl-x_L together with other 2 mice without any hematologic abnormality (Figure 6B filled symbols), showed gradual expansion of leukocytes coexpressing Mac1 and B220 cells from 24 to 32 weeks after transplantation (Figure 6B left panel). In particular, one mouse represented as open diamonds in the right panel of Figure 6B showed a strong leukocytosis from 36 weeks after transplantation.

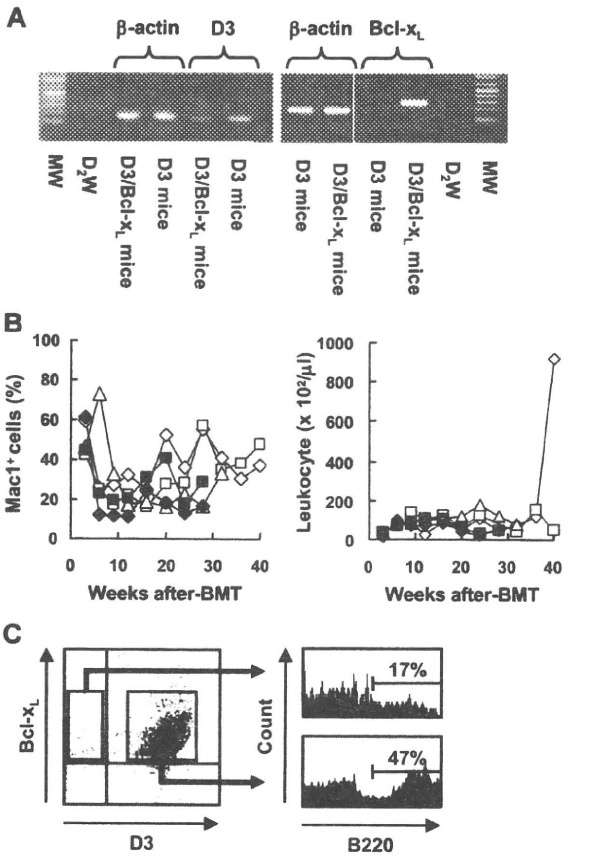

Figure 6. Hematologic abnormality in mice that received transplants of KL cells genetically modified to express D3 and Bcl-x_L. (A) RT-PCR analysis of D3 and Bcl-x_L expression in peripheral blood cells from mice that underwent transplantation with D3-transduced or D3- and Bcl-x_L–transduced KL cells. Left and right panels show D3 and Bcl-x_L expression, respectively. β-actin is used as an internal control. D3 mice indicates mice that received transplants of D3-transduced KL cells; D3/Bcl-x_L mice, mice that received transplants of D3- and Bcl-x_L–transduced KL cells; and MW, molecular weight marker. A vertical line has been inserted to indicate repositioned gel lanes of β-actin and Bcl-X_L. (B-C) A total of 5 mice received transplants of KL cells transduced with both D3 and Bcl-x_L. The percentages of leukocytes expressing Mac1 (B) and the total number of leukocytes (C) in the peripheral blood are shown. Each open or filled symbol represents a mouse with or without hematologic abnormality, respectively.

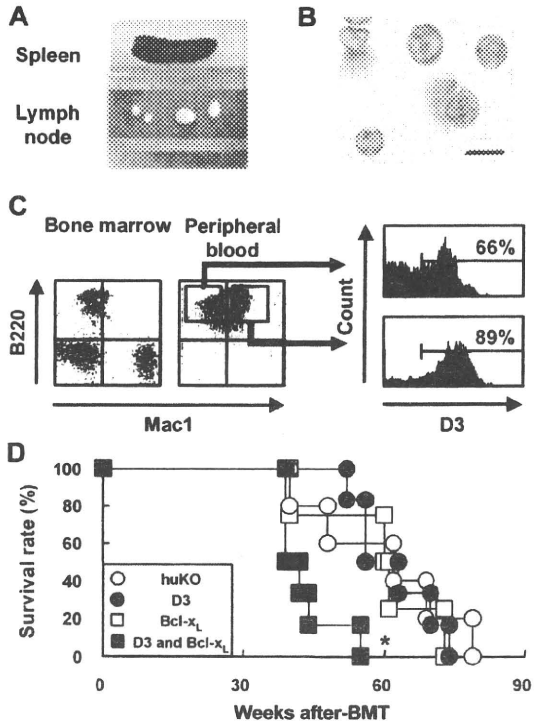

Figure 7. Analysis of mice affected with B lymphoma after transplantation with D3- and Bcl-x_L–transduced KL cells. (A-B) Morphologic appearance of spleen, lymph nodes (A), and peripheral blood cells (May-Gruenwald-Giemsa staining; B) in mice that received transplants of D3- and Bcl-x_L–transduced KL cells at 40 weeks after transplantation (63×/1.4 NA oil objective). Bar in panel B represents 10 mm. (C) Flow cytometric analysis of marrow or peripheral blood cells (left and middle panels, respectively). D3 expression in $Mac1^-$ or $Mac1^+$ cells in $B220^+$ population was further analyzed (right panel). (D) Survival analysis of mice that underwent transplantation with huKO-transduced (○), D3-transduced (●), Bcl-x_L–transduced (□), or D3- and Bcl-x_L–transduced KL cells (■). BMT indicates BM transplantation. *$P < .01$ compared with the other groups.

Characterization of cells transduced with D3 and Bcl-x_L

In 1 of the 3 mentioned mice that displayed a proliferation of $Mac1^+/B220^+$ cells, the population of cells expressing both D3 and Bcl-x_L on their surfaces dominated that of cells expressing Bcl-x_L alone at 24 weeks after transplantation (Figure 6C). Whereas 17% of cells expressing Bcl-x_L alone were positive for B220, almost half of the cells expressing both D3 and Bcl-x_L showed high-level expression of B220 (Figure 6C). Furthermore, another of the mice that underwent transplantation with D3- and Bcl-x_L–transduced KL cells exhibited body weight loss, low activity levels, hunched posture, splenomegaly, and lymph node swelling (Figure 7A) as well as abnormal hematologic values, including leukocytosis (white blood cells, 9.5×10^4/mL), severe anemia (red blood cells, 5.4×10^4/mL), and thrombocytopenia (platelets, 6.9×10^4/mL) with atypical lymphocytes, at 40 weeks after transplantation (Figures 6B,7B and data not shown). Flow cytometric analysis revealed that cells expressing both B220 and Mac1 proliferated in the peripheral blood, spleen, and lymph nodes, but not in the BM; the proliferated cells expressing both B220 and Mac1 had higher levels of expression of D3 on their surfaces than cells expressing only B220 (Figure 7C). Mice that underwent transplantation with both D3- and Bcl-x_L–transduced KL cells (filled squares in Figure 7D) had shorter survival curves than mice that underwent transplantation with cells transduced with huKO, D3, or Bcl-x_L (Figure 7D; $P < .01$, D3 and Bcl-x_L compared with the other groups).

Gene expression profiling of the lymphoma

The correlation of coefficients of the expression profiles between each of the 2 lymphoma cell lines and the controls were 0.990 (L1) and 0.964 (L2), indicating that the lymphoma cell lines harbored similar global gene expression patterns, although they were established independently. Among 41 278 probes, 19 282 (L1, 12 532 nonredundant [nr] genes) or 18 320 (L2, 11 827 nr genes) exhibited signal values more than 100 in the lymphoma or controls. The number of genes that were up- or down-regulated in the lymphoma was 3354 (25.9% of the 12 532 nr genes; L1) or 3243 (27.4% of 11 827 nr genes; L2). Gene Ontology analysis of the results of the top 10% of the up- or down-regulated genes (1182 and 1253, respectively) showed that genes related to "cell cycle," "mitosis," and "amino acid/amine metabolic processes" were abundant among the up-regulated genes, whereas mainly those related to "immune response" were abundant among the "down-regulated genes" (supplemental Tables 1-2). Transcription of the *D3* gene in lymphoma was approximately twice that in normal splenocytes.

Discussion

We demonstrated one of the possible mechanisms by which hematologic malignancies can develop in vivo by characterizing a B-cell lymphoma that developed spontaneously in mice derived from retrovirally transduced ES cells. The mice and their progeny with a single copy of the provirus integrated in the D3 locus showed preferential proliferation of the B-cell lineage and finally died of malignant B-cell lymphoma. We showed that although dopamine signaling through D3 induced HPCs to differentiate preferentially into pre-B cells, this stimulation was insufficient for spontaneous development of lymphoma, which needed the additional expression of the Bcl-x_L gene. Taken together, these results suggest that the lymphoma caused by deregulation of D3 expression is an example of cancer developing in accordance with the "2-hit" theory.

One of the key questions in gene therapy is whether retroviral integration per se is sufficient for leukemogenesis. As shown in clinical trials up to the present, retroviruses are integrated near actively transcribed regions and sometimes cause leukemogenesis by the activation of proto-oncogenes near the integration sites. However, recent studies have shown that leukemia cells in SCID-X1 patients carry additional genetic changes, such as a gain-of-function mutation in *NOTCH*, deletion of the tumor suppressor gene locus cyclin-dependent kinase 2A (*CDKN2A*), *STIL-TAL1* rearrangement, and 6q interstitial losses, suggesting that the leukemia observed in SCID-X1 cases develops in accordance with multistep tumorigenesis theory.[7,8]

Gilliland[27] proposed that, as is often the case with solid tumors, hematologic malignancies are also subject to the "2-hit" theory.[28] They suggested that hematologic malignancy results from sequential mutations of class I genes (genes for proliferation and/or survival advantage) and class II genes (differentiation-related genes). If this is the case, then the presence of the provirus at the D3 locus represented the mutation of a class II gene (overexpression of the *D3* gene), and other genetic changes that function as class I genes should be required for lymphoma transformation. Although these class I genes remain unidentified, it is highly likely that they are related to cell cycle–associated molecules such as cyclin D1,[29] or the cyclin-dependent kinase inhibitors $p14^{ARF}$ and $p16^{INK4a}$,[30] or that they are oncogenes such as c-Myc and Ras family genes,[31-33] or

antiapoptotic genes such as Bcl-x_L.[33,34] Indeed, our microarray-based gene expression profiling revealed that several genes were up- or down-regulated in the lymphoma cell lines. In particular, it should be noted that several genes related to "cell cycle," such as *CDKN2A*, *CDKN2B*, and *Trp63* (p63), were highly up-regulated in the lymphoma.

Although the results were reminiscent of the mechanism by which leukemia develops in human SCID-X1 cases, why was the substantial amount of time needed for the development of lymphoma in vivo? Baum et al said that malignant transformation is not a necessary consequence of insertional proto-oncogene up-regulation but results from a complex series of multiple factors (eg, the genes conferring the selective advantage on gene-corrected cells, the culture conditions favoring expansion of promalignant clones, and the engraftment conditions generating stress hematopoiesis, associated with an antiapoptotic cytokine milieu that might favor the selection of pretransformed mutants).[35] Given that EGFP did not give rise to such selective advantage, gene-modified ES cells were cultured without any strong selective pressure, and the very limited numbers of transduced ES cells (< 10 cells) were used to generate transgenic mice; however, the probability of lymphomagenesis in the present study has been considered to be extremely low. Therefore, the substantial amount time might account for a pause needed for the occurrence of other genetic mutations in pre–B-cell lineage that proliferated slowly by the aberrant expression of D3.

To our knowledge, there have been no reports of B-cell lymphoma related to the aberrant expression of D3. D3 is one of 5 7-transmembrane G protein–coupled receptors, referred to as D1 to D5, all of which influence cell biology by modulating adenylate cyclase; typically, the D1 subfamily, containing D1 and D5, stimulates adenylate cyclase and forms cyclic AMP, whereas the D2 subfamily, containing D2, D3, and D4, inhibits adenylate cyclase and modulates Ca^{2+} signaling by inhibiting Ca^{2+} entry through voltage-sensitive Ca^{2+} channels.[22] Numerous studies have elucidated the constant communication between the nervous and immune systems, and the existence of dopamine receptors on lymphocytes has been analyzed by RT-PCR,[36] by the binding assay using dopamine ligands,[37] and by immunostaining using specific antibodies.[38] According to the results, which are still inconclusive, murine and human B cells, unlike T lymphocytes, hardly express D3. Although one paper has described the cytostatic effect of dopamine on cycling B cells such as lymphoma cell lines, the effect was independent of dopamine receptors, and oxidative stress constituted the primary mechanisms.[39] Considering the fact that neurotransmitters, including dopamine, elicit various functions in T cells via their receptors (including proliferation, adhesion, and cytokine secretion), B cells, if forced to express excessive D3, would be subjected to the multiple effects of dopamine, some of which would induce the proliferation of pre-B cells.

Our study also contributes information on the issue of the safety of vectors used in gene therapy clinical trials. Recently, vectors carrying weaker promoter/enhancer units than in the wild-type of retroviral LTRs have been suggested as safer gene transfer tools for use in clinical trials.[40] In keeping with this, Modlich et al, using a very sophisticated assay, reported that lentiviral vectors were much safer than gammaretroviral vectors in transformation of primary hematopoietic cells.[41] They also suggested altering the vector's enhancer-promoter elements (eg, by using the target gene's own promoter element for the new vector design). As shown in our study, however, such vectors also need to be integrated into the host genome to express the therapeutic gene—an action that can be seen as a possible "first hit" toward leukemogenesis. Therefore, we should be aware that even self-inactivating lentiviral vectors,[42] which are constructed by deletion of the U3 region in the 3′ LTR, with genetic insulator elements,[43] can be liable to cause hematologic malignancies. The need remains to develop other types of vectors for the correction of mutated genes.

Acknowledgments

We thank Dr Richard C. Mulligan (Harvard Medical School) for providing 293gpg, Shin-Ichi Nishikawa (RIKEN, the Center for Developmental Biology) for providing PA6, K. Hata and K. Nakabayashi for analyzing the microarray data, and Dr F. Candotti for providing a critical review of the manuscript. We also thank Ms Naoko Okano and Junko Zenkoh for their excellent secretarial assistance.

This work was supported by grants from the Ministry of Education, Culture, Sports, Science and Technology of Japan, and the Ministry of Health, Labor and Welfare of Japan (M.O.).

Authorship

Contribution: Y.H. and S.H. performed the experiments; and Y.H. and M.O. designed the research.

Conflict-of-interest disclosure: The authors declare no competing financial interests.

Correspondence: Masafumi Onodera, Department of Genetics, National Research Institute for Child Health and Development, 2-10-1 Okura, Setagaya-ku, Tokyo 157-8575, Japan; e-mail: monodera@nch.go.jp.

References

1. Aiuti A, Cattaneo F, Galimberti S, et al. Gene therapy for immunodeficiency due to adenosine deaminase deficiency. *N Engl J Med.* 2009; 360(5):447-458.
2. Hacein-Bey-Abina S, Le Deist F, Carlier F, et al. Sustained correction of X-linked severe combined immunodeficiency by ex vivo gene therapy. *N Engl J Med.* 2002;346(16):1185-1193.
3. Ott MG, Schmidt M, Schwarzwaelder K, et al. Correction of X-linked chronic granulomatous disease by gene therapy, augmented by insertional activation of MDS1-EVI1, PRDM16 or SETBP1. *Nat Med.* 2006;12(4):401-409.
4. Cartier N, Hacein-Bey-Abina S, Bartholomae CC, et al. Hematopoietic stem cell gene therapy with a lentiviral vector in X-linked adrenoleukodystrophy. *Science.* 2009;326(5954):818-823.
5. Baum C, Düllmann J, Li Z, et al. Side effects of retroviral gene transfer into hematopoietic stem cells. *Blood.* 2003;101(6):2099-2113.
6. Nienhuis AW, Dunbar CE, Sorrentino BP. Genotoxicity of retroviral integration in hematopoietic cells. *Mol Ther.* 2006;13(6):1031-1049.
7. Hacein-Bey-Abina S, Von Kalle C, Schmidt M, et al. LMO2-associated clonal T cell proliferation in two patients after gene therapy for SCID-X1. *Science.* 2003;302(5644):415-419.
8. Howe SJ, Mansour MR, Schwarzwaelder K, et al. Insertional mutagenesis combined with acquired somatic mutations causes leukemogenesis following gene therapy of SCID-X1 patients. *J Clin Invest.* 2008;118(9):3143-3150.
9. Hacein-Bey-Abina S, Garrigue A, Wang GP, et al. Insertional oncogenesis in 4 patients after retrovirus-mediated gene therapy of SCID-X1. *J Clin Invest.* 2008;118(9):3132-3142.
10. Sanuki S, Hamanaka S, Kaneko S, et al. A new red fluorescent protein that allows efficient marking of murine hematopoietic stem cells. *J Gene Med.* 2008;10(9):965-971.
11. Suzuki A, Obi K, Urabe T, et al. Feasibility of ex vivo gene therapy for neurological disorders using the new retroviral vector GCDNsap packaged in the vesicular stomatitis virus G protein. *J Neurochem.* 2002;82(4):953-960.
12. Hamanaka S, Nabekura T, Otsu M, et al. Stable

transgene expression in mice generated from retrovirally transduced embryonic stem cells. *Mol Ther.* 2007;15(3):560-565.

13. Swendeman SL, Spielholz C, Jenkins NA, Gilbert DJ, Copeland NG, Sheffery M. Characterization of the genomic structure, chromosomal location, promoter, and development expression of the alpha-globin transcription factor CP2. *J Biol Chem.* 1994;269(15):11663-11671.
14. Iwama A, Osawa M, Hirasawa R, et al. Reciprocal roles for CCAAT/enhancer binding protein (C/EBP) and PU. 1 transcription factors in Langerhans cell commitment. *J Exp Med.* 2002;195(5):547-558.
15. Ory DS, Neugeboren BA, Mulligan RC. A stable human-derived packaging cell line for production of high titer retrovirus/vesicular stomatitis virus G pseudotypes. *Proc Natl Acad Sci U S A.* 1996;93(21):11400-11406.
16. Kodama H, Sudo H, Koyama H, Kasai S, Yamamoto S. In vitro hemopoiesis within a microenvironment created by MC3T3-G2/PA6 preadipocytes. *J Cell Physiol.* 1984;118(3):233-240.
17. Schmidt M, Zickler P, Hoffmann G, et al. Polyclonal long-term repopulating stem cell clones in a primate model. *Blood.* 2002;100(8):2737-2743.
18. National Center for Biotechnology Information. Mouse Genome Database. Available at http://www.ncbi.nlm.nih.gov. Accessed January 10, 2007.
19. Huang DW, Sherman BT, Lempicki RA. Systematic and integrative analysis of large gene lists using DAVID bioinformatics resources. *Nat Protoc.* 2009;4(1):44-57.
20. Dennis G Jr, Sherman BT, Hosack DA, et al. DAVID: database for annotation, visualization, and integrated discovery. *Genome Biol.* 2003;4(5):P3.
21. Mizutani T, Ito T, Nishina M, Yamamichi N, Watanabe A, Iba H. Maintenance of integrated proviral gene expression requires Brm, a catalytic subunit of SWI/SNF complex. *J Biol Chem.* 2002;277(18):15859-15864.
22. Missale C, Nash SR, Robinson SW, Jaber M, Caron MG. Dopamine receptors: from structure to function. *Physiol Rev.* 1998;78(1):189-225.
23. Watanabe Y, Nakayama T, Nagakubo D, et al. Dopamine selectively induces migration and homing of naive $CD8^+$ T cells via dopamine receptor D3. *J Immunol.* 2006;176(2):848-856.
24. Snider SR, Kuchel O. Dopamine: an important neurohormone of the sympathoadrenal system: significance of increased peripheral dopamine release for the human stress response and hypertension. *Endocr Rev.* 1983;4(3):291-309.
25. Hasko G, Szabo C. Regulation of cytokine and chemokine production by transmitters and cotransmitters of the autonomic nervous system. *Biochem Pharmacol.* 1998;56(9):1079-1087.
26. Weihe E, Nohr D, Michel S, et al. Molecular anatomy of the neuro-immune connection. *Int J Neurosci.* 1991;59(1-3):1-23.
27. Gilliland DG. Hematologic malignancies. *Curr Opin Hematol.* 2001;8(4):189-191.
28. Hanahan D, Weinberg RA. The hallmarks of cancer. *Cell.* 2000;100(1):57-70.
29. Bodrug SE, Warner BJ, Bath ML, Lindeman GJ, Harris AW, Adams JM. Cyclin D1 transgene impedes lymphocyte maturation and collaborates in lymphomagenesis with the myc gene. *EMBO J.* 1994;13(9):2124-2130.
30. García MJ, Martínez-Delgado B, Cebrian A, Martínez A, Benítez J, Rivas C. Different incidence and pattern of p15INK4b and p16INK4a promoter region hypermethylation in Hodgkin's and CD30-positive non-Hodgkin's lymphomas. *Am J Pathol.* 2002;161(3):1007-1013.
31. Hermann M, Scholman HJ, Marafioti T, Stein H, Schriever F. Differential expression of apoptosis, Bcl-x and c-Myc in normal and malignant lymphoid tissues. *Eur J Haematol.* 1997;59(1):20-30.
32. Lazarus AH, Kawauchi K, Rapoport MJ, Delovitch TL. Antigen-induced B lymphocyte activation involves the p21ras and ras.GAP signaling pathway. *J Exp Med.* 1993;178(5):1765-1769.
33. Swanson PJ, Kuslak SL, Fang W, et al. Fatal acute lymphoblastic leukemia in mice transgenic for B cell-restricted bcl-xL and c-myc. *J Immunol.* 2004;172(11):6684-6691.
34. Pallis M, Zhu YM, Russell NH. Bcl-x(L) is heterogeneously expressed by acute myeloblastic leukaemia cells and is associated with autonomous growth in vitro and with P-glycoprotein expression. *Leukemia.* 1997;11(7):945-949.
35. Baum C, Kustikova O, Modlich U, Li Z, Fehse B. Mutagenesis and oncogenesis by chromosomal insertion of gene transfer vectors. *Hum Gene Ther.* 2006;17(3):253-263.
36. Nagai Y, Ueno S, Saeki Y, Soga F, Yanagihara T. Expression of the D3 dopamine receptor gene and a novel variant transcript generated by alternative splicing in human peripheral blood lymphocytes. *Biochem Biophys Res Commun.* 1993;194(1):368-374.
37. Ricci A, Veglio F, Amenta F. Radioligand binding characterization of putative dopamine D3 receptor in human peripheral blood lymphocytes with [3H]7-OH-DPAT. *J Neuroimmunol.* 1995;58(2):139-144.
38. McKenna F, McLaughlin PJ, Lewis BJ, et al. Dopamine receptor expression on human T- and B-lymphocytes, monocytes, neutrophils, eosinophils and NK cells: a flow cytometric study. *J Neuroimmunol.* 2002;132(1-2):34-40.
39. Meredith EJ, Holder MJ, Rosén A, et al. Dopamine targets cycling B cells independent of receptors/transporter for oxidative attack: implications for non-Hodgkin's lymphoma. *Proc Natl Acad Sci U S A.* 2006;103(36):13485-13490.
40. Yi Y, Hahm SH, Lee KH. Retroviral gene therapy: safety issues and possible solutions. *Curr Gene Ther.* 2005;5(1):25-35.
41. Modlich U, Navarro S, Zychlinski D, et al. Insertional transformation of hematopoietic cells by self-inactivating lentiviral and gammaretroviral vectors. *Mol Ther.* 2009;17(11):1919-1928.
42. Miyoshi H, Blömer U, Takahashi M, Gage FH, Verma IM. Development of a self-inactivating lentivirus vector. *J Virol.* 1998;72(10):8150-8157.
43. Emery DW, Yannaki E, Tubb J, Nishino T, Li Q, Stamatoyannopoulos G. Development of virus vectors for gene therapy of beta chain hemoglobinopathies: flanking with a chromatin insulator reduces gamma-globin gene silencing in vivo. *Blood.* 2002;100(6):2012-2019.

Hum Genet (2010) 127:619–628
DOI 10.1007/s00439-010-0822-7

REVIEW ARTICLE

Molecular pathogenesis of a novel mutation, G108D, in short-chain acyl-CoA dehydrogenase identified in subjects with short-chain acyl-CoA dehydrogenase deficiency

Kenichiro Shirao · Satoshi Okada · Go Tajima · Miyuki Tsumura · Keiichi Hara · Shin'ichiro Yasunaga · Motoaki Ohtsubo · Ikue Hata · Nobuo Sakura · Yosuke Shigematsu · Yoshihiro Takihara · Masao Kobayashi

Received: 22 February 2010 / Accepted: 30 March 2010 / Published online: 8 April 2010

Abstract Short-chain acyl-CoA dehydrogenase (SCAD) is a mitochondrial enzyme involved in the β-oxidation of fatty acids. Genetic defect of SCAD was documented to cause clinical symptoms such as progressive psychomotor retardation, muscle hypotonia, and myopathy in early reports. However, clinical significance of SCAD deficiency (SCADD) has been getting ambiguous, for some variants in the *ACADS* gene, which encodes the SCAD protein, has turned out to be widely prevailed among general populations. Accordingly, the pathophysiology of SCADD has not been clarified thus far. The present report focuses on two suspected cases of SCADD detected through the screening of newborns by tandem mass spectrometry. In both subjects, compound heterozygous mutations in *ACADS* were detected. The mutated genes were expressed in a transient gene expression system, and the enzymatic activities of the obtained mutant SCAD proteins were measured. The activities of the mutant SCAD proteins were significantly lower than that of the wild-type enzyme, confirming the mechanism underlying the diagnosis of SCADD in both subjects. Moreover, the mutant SCAD proteins gave rise to mitochondrial fragmentation and autophagy, both of which were proportional to the decrease in SCAD activities. The association of autophagy with programed cell death suggests that the mutant SCAD proteins are toxic to mitochondria and to the cells in which they are expressed. The expression of recombinant *ACADS*-encoded mutant proteins offers a technique to evaluate both the nature of the defective SCAD proteins and their toxicity. Moreover, our results provide insight into possible molecular pathophysiology of SCADD.

K. Shirao and S. Okada contributed equally to this work.

Nucleotide sequence data reported are available in the DDBJ database under the accession number AB527081.

Electronic supplementary material The online version of this article (doi:10.1007/s00439-010-0822-7) contains supplementary material, which is available to authorized users.

K. Shirao · S. Okada · G. Tajima (✉) · M. Tsumura · K. Hara · M. Kobayashi
Department of Pediatrics, Hiroshima University Graduate School of Biomedical Sciences, 1-2-3 Kasumi, Minami-ku, Hiroshima 734-8551, Japan
e-mail: acadugo@mac.com

S. Yasunaga · M. Ohtsubo · Y. Takihara
Department of Stem Cell Biology, Research Institute for Radiation Biology and Medicine, Hiroshima University, Hiroshima 734-8553, Japan

I. Hata
Department of Pediatrics, Faculty of Medical Sciences, University of Fukui, Fukui 910-1193, Japan

N. Sakura
Nursing House for Severe Motor and Intellectual Disabilities "Suzugamine", Hiroshima 731-5122, Japan

Y. Shigematsu
Department of Health Science, Faculty of Medical Sciences, University of Fukui, Fukui 910-1193, Japan

Introduction

Short-chain acyl-CoA dehydrogenase (SCAD), a mitochondrial enzyme of the fatty acid β-oxidation system, mediates the metabolic transition from acyl-CoA with four- or six-carbon chains to 2-enoyl-CoA in the first step of the β-oxidation spiral. SCAD deficiency (SCADD) occurs as a rare autosomal recessive disorder, first reported in 1985 (Amendt et al. 1987; Bennett et al. 1985; Coates et al.

1988). The clinical symptoms such as progressive psychomotor retardation, muscle hypotonia, and myopathy were documented (Bhala et al. 1995; Corydon et al. 2001). As the results of the enzymatic defects, increased levels of C_4-acylcarnitine in peripheral blood and ethylmalonic acid (EMA) in urine are observed.

Acylcarnitine measurement using tandem mass spectrometry (MS/MS) is a new screening technology that has been applied to the detection of inborn errors of organic acid and fatty acid metabolism in newborns, including those with symptomatic and asymptomatic SCADD as well as their asymptomatic siblings (Bok et al. 2003; Naito et al. 1989b; Pedersen et al. 2008). This has led to the recognition that in the general population, many individuals may carry *ACADS* mutations but lack SCADD-related symptoms. Precise knowledge of the pathogenesis, natural course, and prognosis of SCADD, based on a definitive diagnosis, is essential for promoting a better understanding about SCADD and for developing an even more efficient screening system.

Mutations in the *ACADS* gene, which encodes the SCAD protein, have been identified in symptomatic patients with SCADD. Overall, approximately 60 mutations in *ACADS* are known thus far (Gregersen et al. 2008). These may result in an insufficient energy supply during β-oxidation, especially under conditions of starvation or stress, thereby triggering the onset of SCADD (Gregersen et al. 2001). Indeed, two studies reported a correlation between *ACADS* mutations and the deterioration of SCAD enzymatic activities (Naito et al. 1989a, b). However, the residual enzymatic activities documented in those studies were, in many patients, too high to allow a definitive diagnosis of SCADD although this may have been due to the overlapping activity of MCAD toward C4–C6 acyl-CoAs (Wanders et al. 1999).

Two common *ACADS* sequence variants, R171W (511C>T) and G209S (625G>A), have been identified in healthy populations at a frequency of 14–30% (Corydon et al. 1996, 2001; Gregersen et al. 1998; Pedersen et al. 2008). Genetic analysis of patients with elevated levels of ethylmalonate in the urine revealed that approximately 69% was homozygous or compound heterozygous for these variants (Gregersen et al. 2001). Although neither of the variants seems to be sufficient to cause disease, it cannot be ruled out that expression of either one may nonetheless contribute to disease pathogenesis in conjunction with other, hitherto unknown factors (van Maldegem et al. 2006). Thus, whether mutations in *ACADS* are related directly to the deterioration of short-chain fatty acid oxidation and to the clinical symptoms of SCADD remain controversial.

In this study, we identified the first two cases of SCADD in Japan, including one subject with a novel *ACADS* G108D mutation. Analysis of the recombinant SCAD mutant proteins showed that all of them give rise to a severe decrease in SCAD enzymatic activity. Furthermore, differences in the solubility, degree of mitochondrial fragmentation, and autophagy were identified among SCAD wild-type (WT), mutant, and variant proteins. Together with recent studies in which a correlation between mitochondrial fragmentation and neurodegeneration was demonstrated (Knott et al. 2008), our findings may provide an important clue regarding the molecular mechanism underlying SCADD and the neuronal symptoms possibly associated with the disease.

Materials and methods

Case report

Newborns with metabolic disorders of organic and fatty acids have been screened in Hiroshima using MS/MS technology since 1999. Based on the screening results, two females suspected of having SCADD were identified from among the more than 200,000 infants screened. In these two subjects, high levels of C_4-acylcarnitine were detected in blood spotting by MS/MS, and the level of ethylmalonic acid excreted in urine was elevated as well (Sup. Table 1). According to these criteria, the subjects were susceptible to SCADD; however, the children, who are now 4-year-old, have thus far not shown any symptom related to SCADD, and neither do the members of their families.

Blood samples were obtained from the subjects and from healthy adult controls after they provided written informed consent. The study was approved by the Ethics Committee/ Internal Review Board of Hiroshima University.

Molecular genetics

Genomic DNA was extracted from peripheral white blood cells. All of the exons and flanking introns comprising the *ACADS* gene were PCR-amplified using the primers listed in Sup. Table 2. The PCR products were sequenced directly using a BigDye Terminator v3.1 cycle sequencing kit (Applied Biosystems, Foster City, CA, USA) and an ABI PRISM 310 genetic analyzer (Applied Biosystems).

Total RNA was extracted from the cells using ISOGEN (Nippon Gene Co., Tokyo, Japan), and the cDNA was synthesized from 5 μg of total RNA using a SuperScript first-strand synthesis system for RT-PCR (Invitrogen, Carlsbad, CA, USA). PCR of the WT and mutant alleles was carried out with primers that spanned the entire *ACADS* coding region. The PCR products were cloned into pGEM-T Easy vector (Promega, Madison, WI, USA). The three mutants were generated by PCR-based mutagenesis of the WT construct using the mismatched PCR primers listed in

Sup. Table 2. These fragments were subcloned into the *Eco*RI and *Xho*I sites of the mammalian expression vector PcDNA myc-His (+) (Invitrogen).

Analysis of gene expression

The SCAD dehydrogenase activity targeting C4-CoA is maximal in the mitochondrial fatty acid cycle, but similar enzymatic activity, at comparable levels, is expressed by MCAD in a reaction involving the same substrate (Coates et al. 1988; Wanders et al. 1999). Thus, in studies examining SCAD enzymatic activities, MCAD enzymatic activity was neutralized by pre-treating fibroblasts, lymphocytes, and muscle samples with a polyclonal antibody against the latter protein; nonetheless, SCAD enzymatic activities varied greatly (Corydon et al. 1997; 2001; Gregersen et al. 1998; Naito et al. 1989b; Tein et al. 2008). Therefore, it is unclear whether the in vitro data obtained in those studies of SCADD patients reflected only SCAD, and not MCAD, activity. Initially, we also tried to measure cellular SCAD enzymatic activity by pre-treating the cells with a polyclonal antibody against MCAD, but, likewise, the data were not convincing. Therefore, we devised a transient gene expression system that overcame the contaminating influence of MCAD.

HEK293 cells were maintained in DMEM containing 10% fetal calf serum (FCS) (HyClone, Logan, UT, USA), 100 U penicillin/ml, and 100 μg streptomycin/ml. At 24 h before transfection, the cells were harvested by trypsinization and replated at a density of 1×10^6 cells/ml in 100-mm culture dishes. Plasmid DNA (5 μg per plate) carrying the WT, P55L, G108D, E344G, R171W, or G209S alleles of *ACADS* was introduced into HEK293 cells by calcium phosphate-mediated transfection.

Enzymatic activity assays were carried out at 24 h post-transfection using 2×10^5 cells from each plate and following a previously reported method, with some modification (Tajima et al. 2005). In brief, the reaction mixture contained 80 mM K_2HPO_4 (pH 7.0), 1 mM *n*-butyryl-CoA (Sigma Chemical, St. Louis, MO, USA), 2 mM phenazine methosulfate (Nacalai Tesque, Tokyo, Japan), 0.1 mM flavin adenine dinucleotide, and the cell lysate. After incubation at 37°C for 5 min, the reactions were terminated by the addition of 0.3 mM $HClO_4$. The denatured proteins were centrifuged, and the supernatant introduced into a high-performance liquid chromatography (HPLC) system set up to detect crotonyl-CoA production based on its UV absorption at 260 nm. A linear increase of crotonyl-CoA production was detected within the range of 0.5×10^5–3.0×10^5 HEK293 cells; thus, in subsequent experiments, extracts were prepared from 2×10^5 HEK293 cells. The same assays were carried out at 26 and 41°C incubation temperatures.

The remainder of the cell extracts was used for Western blotting, in which the SCAD protein was detected using anti-Myc antibodies.

Separation of the SCAD proteins into soluble and insoluble fractions

Plasmids carrying the WT, P55L, G108D, E344G, R171W, or G209S *ACADS* alleles were introduced into HEK293 cells by calcium phosphate-mediated transfection. At 24 h post-transfection, 5×10^5 cells from each plate were transferred to 1.5-ml Eppendorf tubes and washed with 1× PBS. The cells were treated with extraction buffer (10% glycerol, 0.15 mM KCl, 1.5 mM MgCl2, 1 mM EDTA, 0.5% Triton X-100, 20 mM HEPES, with protease inhibitor), vortexed, and then set on ice for 10 min, followed by centrifugation (17,000×*g*, 10 min, 4°C) to isolate the soluble and insoluble fractions. Since SCAD mutant proteins have a tendency to misfold and aggregate, they are predominately contained in the insoluble fraction (Pedersen et al. 2003). WT proteins and proteins encoded by the common variants are found almost in the soluble fraction. Accordingly, both the supernatants, as the soluble fraction, and the pellets, as the insoluble fraction, were analyzed by Western blotting.

Immunostaining of the SCAD proteins

The U2-OS cells were maintained in DMEM containing 10% fetal calf serum (FCS) (HyClone, Logan, Utah, USA), 100 U penicillin/ml, and 100 μg streptomycin/ml. At 24 h before transfection, the cells were harvested by trypsinization and replated at a density of 2×10^5 cells/ml in 35-mm culture dishes with a cover glass. Plasmid DNA (1 μg per plate) carrying the WT, P55L, G108D, E344G, R171W, or G209S *ACADS* alleles were introduced into U2-OS cells by lipofection using lipofectamine 2000 according to the manufacturer's guidelines (Invitrogen). The cells were stained 24 h post-transfection with an anti-c-Myc rabbit polyclonal IgG (200 μg/ml; Santa Cruz Biotechnology) and an Alexa Fluor 488 goat anti-rabbit IgG (2 mg/ml; Molecular Probes) for SCAD proteins, Hoechst 33342 1 μg/ml (Calbiochem) for nuclei, and MitoTracker Red CM-H_2XRos (Molecular Probes) for mitochondria. Images were taken using an OLYMPUS microscope BX50 equipped with DP70. Stained cells were photographed at the same exposure time for each dye to allow comparison.

Mitochondrial fragmentation data were evaluated statistically and expressed as the means and SE. Experiments were performed in triplicate and repeated at least three times. Statistical analysis was carried out using Student's *t* tests; $^{**}p < 0.01$; $^{***}p < 0.001$.

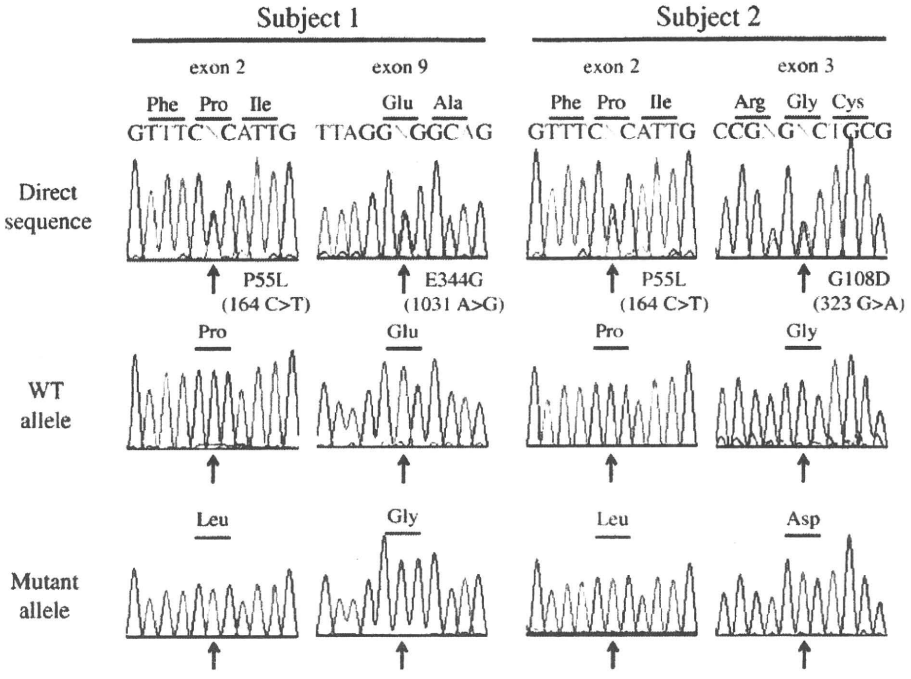

Fig. 1 Sequence analysis of *ACADS*. Genomic DNAs of *ACADS* from the two subjects who positively screened for SCADD were amplified by PCR, and the products were sequenced by direct sequencing. Sequencing analysis revealed compound heterozygous *ACADS* mutations in both subjects. *Upper row* shows each of sequence of the mutations; Subject 1: Pro55Leu (164C>T) in exon 2 and Glu344Gly (1031A>G) in exon 9; subject 2: Pro55Leu (164C>T) in exon 2 and Gly108Asp (323G>A) in exon 3. *Middle row* showed WT allele sequences of *ACADS*, and *lower row* showed each mutant allele of the subjects

Autophagy analysis of the SCAD-overexpressing cells

The autophagic activities of cells overexpressing WT or G108D mutant SCAD proteins were analyzed in whole-cell lysates prepared as follows: 1×10^6 U2-OS cells were transfected with 5 μg WT or G108D plasmid DNAs by lipofection. At 24 and 48 h post-transfection, the cells were collected and treated with 2× SDS-PAGE buffer. The resulting lysates of these WT and G108D SCAD-overexpressing cells were analyzed by Western blotting using a polyclonal anti-LC3B antibody (1 mg/ml; NOVUS Biologicals) in order to detect LC3-II expression which is induced by autophagosome formation. As a control, whole-cell lysates were prepared from 1×10^6 U2-OS cells with and without pepstatinA and E64d, both of which inhibit the conversion of LC3-II to LC3-I.

Results

Sequence analysis

High molecular weight DNA was extracted from peripheral blood samples obtained from the two subjects diagnosed with SCADD. Exons and the flanking intron regions of *ACADS* were amplified by PCR (Fig. 1). As shown in Fig. 1, both subjects had missense mutations in the *ACADS* gene: in subject 1, in exons 2 [164 C>T (P55L)] and 9 [1031 A>G (E344G)], and in subject 2, in exons 2 [164 C>T (P55L)] and 3 [323 G>A (G108D)]. The G108D mutation was a novel mutation involving an amino acid (G108) that is highly conserved among *Mus musculus, Danio rerio*, and *Drosophila melanogaster*. The G108D mutation was not detected in 100 unrelated Japanese control individuals, suggesting its potential pathogenic nature.

Because we could not obtain subjects' parents blood sample, the respective cDNAs were prepared and then analyzed by subcloning them into the pGEM-T Easy vector to confirm the mutations. Ten clones were sequenced individually, and in each subject, both mutant alleles were found to be expressed equally (Fig. 1). These results suggest that the two subjects had compound heterozygous mutations in *ACADS*.

SCAD activity analysis

Prior to measuring mutant SCAD enzymatic activity, we confirmed that the assay accurately measured the enzymatic activity of SCAD proteins. Accordingly, *ACADS* cDNA was introduced into a mammalian expression vector, pcDNA, and the resulting expression vector was transfected into HEK293 cells using the calcium phosphate co-precipitation method, as previously reported (Okada et al. 2007). Extracts from 1×10^7 of the transfectants were prepared, and *n*-butyryl-CoA dehydrogenase activity was measured in serially diluted cell samples to obtain a standard curve (Fig. 2a). In HEK293 cells, a linear increase in crotonyl-CoA production was measured in the range of 0.5×10^5–3.0×10^5 cells. Based on the results, extracts from 2×10^5

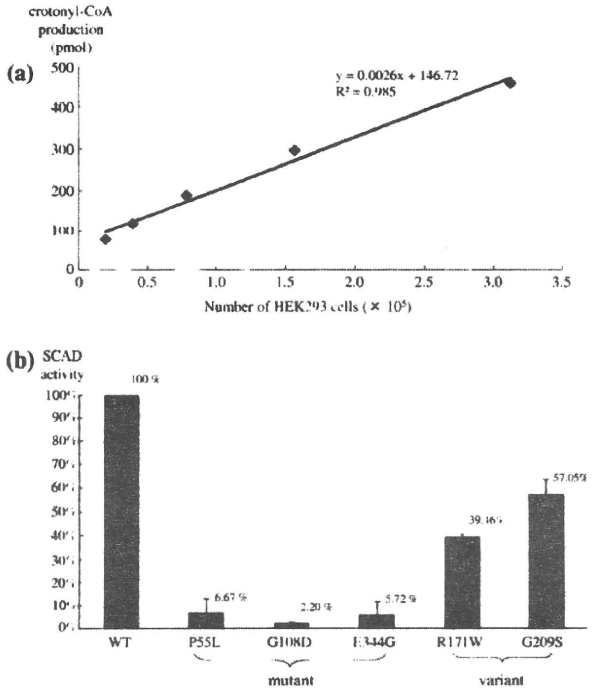

Fig. 2 SCAD enzymatic activity analysis. **a** Butyryl-CoA dehydrogenase activity in crude cell lysates prepared from HEK293 cells transfected with WT *ACADS* plasmid DNA. Standard curve of the enzymatic activity of WT SCAD protein was shown. Based on the results, extracts from 2×10^5 cells were used to analyze SCAD enzymatic activity in all subsequent experiments. **b** SCAD enzymatic activity in HEK293 cells 24 h after transfection with WT or mutant SCAD proteins. WT activity was defined as the 100% value. *Error bars* indicate the standard deviation. The data are the results of triplicate experiments

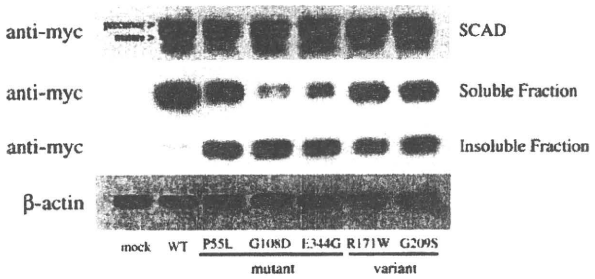

Fig. 3 Western blotting of SCAD proteins. Western blot analysis with an anti-c-Myc antibody to detect SCAD protein. *Top panel* the extracts can be seen to contain equal amounts of SCAD proteins. *Middle* and *lower panels* show the soluble and the insoluble fractions for each of the SCAD proteins. β-Actin served as the control to ensure equal amount of proteins on the filter

cells were used to analyze SCAD enzymatic activity in all subsequent experiments. Each construct was assayed at least three times (Fig. 2b). Expression levels of the recombinant mutant proteins were investigated by Western blot analysis using an anti-c-Myc antibody (Fig. 3).

Compared to the enzymatic activity of the WT SCAD protein, the activities of the G108D and other mutants were <10% (Fig. 2b). The enzymatic profile of the subjects was reproduced by co-transfecting the P55L and E344G mutants (subject 1) or the P55L and G108D mutants (subject 2), and then measuring the enzymatic activities derived from the combined mutant proteins. Low-level activity was detected in each case, analogous to the SCAD activities determined in the subjects (Sup. Fig. 1a). Furthermore, co-transfection of the WT and each of the mutants yielded 60–70% of the normal enzymatic activity, suggesting that these mutants do not influence WT SCAD (data not shown).

Interestingly, an analysis of the common SCAD variants R171W and G209S SCAD showed that their enzymatic activities were 40–60% of the activity measured in the WT (Fig. 2b), whereas co-transfection of R171W and G209S resulted in 50% of the WT activity (Sup. Fig. 1a). According to these results, in individuals harboring these variations, enzymatic activity should be about half that measured in individuals expressing WT SCAD.

In temperature-dependent assay, enzymatic activities of SCAD constructs were entirely lower at 26°C incubation temperature and slightly higher at 41°C incubation temperature than those at 37°C incubation temperature (Sup. Fig. 1b). The whole propensity of decrease of mutants SCAD and variants SCAD against WT SCAD was constant.

Separation of SCAD proteins

To characterize the SCAD mutant proteins, WT, mutant, and variant proteins were purified, and the differences among them were examined. As SCAD mutant proteins are known to misfold and to aggregate (Pedersen et al. 2003) and are thus retained in the insoluble fraction, both the soluble and the insoluble fractions obtained during protein purification were assayed. In the soluble fraction, the amount of mutant SCAD, especially of the G108D mutant, was much less than that determined for the WT (Fig. 3), whereas the amount of variant SCAD in the soluble fraction was only mildly decreased (Fig. 3). As expected, in the insoluble fraction, expression of the mutants was much higher than that of either the WT or the variants (Fig. 3). For each transfectant, the trend was such that the lower the SCAD activity was, the greater was the amount of expression detected in the insoluble fraction.

Immunostaining

Differences in the subcellular localization of the WT and mutant SCAD proteins produced in U2-OS cells were explored by immunostaining. All SCAD proteins were detected in the subcellular region corresponding to the

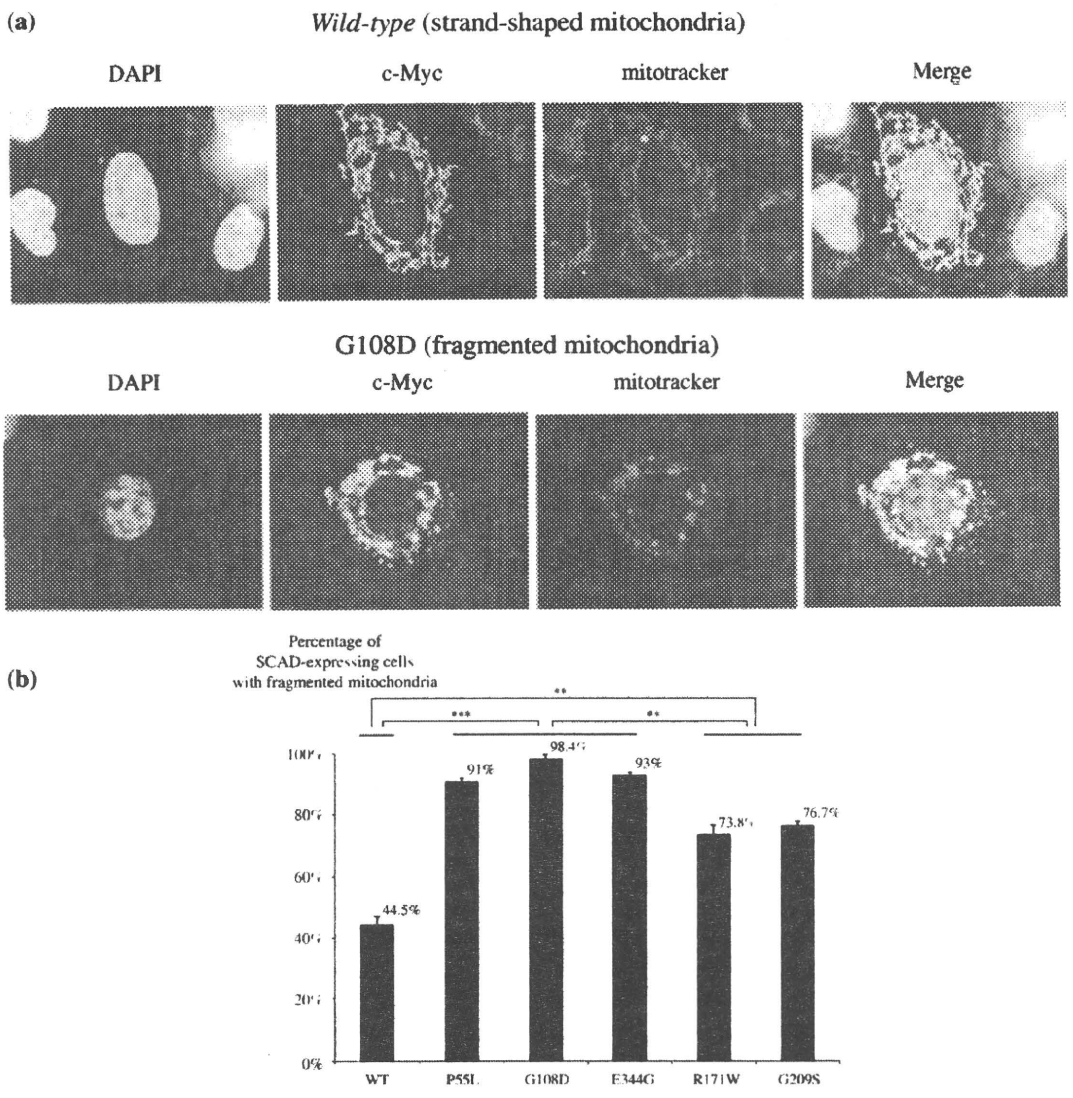

Fig. 4 Immunostaining of WT and G108D SCAD-expressing cells. **a** U2-OS cells transfected with each of the SCAD constructs were immunostained as described in "Materials and methods". Strand-shaped and fragmented mitochondria of cells expressing the WT *ACADS* gene or the G108D mutation were seen, respectively. *Green* showed SCAD protein; *red* showed mitochondria; *blue* showed nuclei. **b** Percentage of SCAD-expressing cells containing fragmented mitochondria. For each transfectant, 300 U2-OS cells were assessed according to mitochondrial shape (***$p < 0.001$, **$p < 0.01$)

mitochondria (Fig. 4a). However, whereas in WT-expressing U2-OS cells, the mitochondria were strand shaped, in cells expressing mutant-SCAD, they were mostly fragmented (Fig. 4a). The mutant proteins were detected in the fragmented mitochondria or spreading within the adjacent cytoplasm. In addition, in many of the mutant-expressing cells the nucleus was deformed. These findings suggest that mutant SCAD proteins are toxic to the mitochondria and/or to the cells themselves (Peng and Jou 2004).

In cells expressing variant SCAD, both strand-shaped and fragmented mitochondria occurred. As in a previous study, the ratio of strand-shaped to fragmented mitochondria was determined in cells containing the WT, mutant, or variant SCAD proteins (Taguchi et al. 2007). The proportion of cells with fragmented mitochondria was much higher in mutant SCAD-expressing cells (Fig. 4b) than in cells expressing the WT (>90 vs. 40%; $p < 0.001$). This trend was strongest in G108D cells and intermediate in the variant cells ($p < 0.01$). These results correlated well with SCAD enzymatic activities, i.e., the lower the SCAD activity of a transfectant was, the higher was the proportion of fragmented mitochondria.

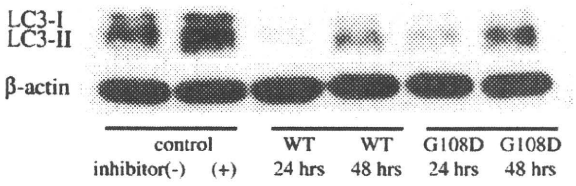

Fig. 5 LC3 assay of WT and G108D SCAD-expressing cells. Western blotting showed that LC3-II, a marker of cellular autophagy, was present in higher amounts in G108D-expressing than in WT-expressing cells. This trend was seen at both 24 and 48 h post-transfection. The amount of protein loaded on the filters was controlled using β-actin

Autophagy in SCAD-overexpressing cells

A recent study showed that mitochondrial fragmentation induces cellular autophagy (Kang and Hwang 2009). Accordingly, we examined whether this was also the case in G108D-expressing cells, in which the severest mitochondrial fragmentation was observed. Autophagy was detected by measuring the expression of LC3-II, a marker of autophagosome formation. At both 24 and 48 h post-transfection, LC3-II expression was stronger in G108D-expressing cells than in cells containing the transfected WT protein (Fig. 5). These results suggested that autophagy was more severely induced in G108D-expressing cells than in those expressing the WT.

Discussion

In this study, compound heterozygous mutations in *ACADS* were identified in two Japanese subjects with SCADD—the first such cases to be diagnosed in Japan. Moreover, in one of them, a novel mutation, G108D, was identified. Enzyme activities of the recombinant mutant SCAD proteins obtained using a transient gene expression system were measured. The activities of the SCAD mutants were found to be <10% of the WT activity (Fig. 2b). Furthermore, co-transfection experiments (P55L and E344G, or P55L and G108D) allowed us to assess the enzymatic activities resulting from the same biallelic mutations detected in the subjects. SCAD activities were also severely impaired in the co-transfectants, showing that the marked SCAD enzymatic defects seen in the two subjects could be precisely measured and characterized by our system. However, to date, neither of these subjects has shown overt clinical symptoms of the disease and, as concluded in previous studies, the genotype–phenotype relationship in SCADD remains unclear. It may well be that the altered SCAD activity may trigger the onset of SCADD under conditions such as starvation or some forms of stress. Therefore, SCADD patients should be followed carefully to obtain a clear understanding of the clinical presentations derived from the enzymatic defect.

The SCAD activities of the R171W and G209S variants were 40–60% in range. Although we also noted an obvious difference in the SCAD activities of the mutants and the variants, the data do not allow us to conclude whether individuals with variant forms of the enzyme will develop clinical symptoms. Another explanation for the pathogenesis of SCADD was proposed by Naito et al. (1989a, b), who suggested that the onset of symptoms is due to the cellular accumulation of abnormal substances (Pedersen et al. 2008). However, it is not known whether, for example, accumulated butyryl-CoA, a substrate of SCAD, or a shortage of its metabolic product plays a role in disease onset, and the pathophysiological implications of the *ACADS* variants and/or mutants remain to be determined.

To further characterize the SCAD mutants and variants, recombinant SCAD proteins were purified, and the soluble and insoluble fractions retained for analysis. The results showed that mutant SCAD proteins were predominately detected in the insoluble fraction, whereas WT protein localized to the soluble fraction (Fig. 3) and variant SCAD was distributed between the two. Generally, the insoluble fraction is considered to contain the cellular bulk of misfolded proteins (Malolepsza 2008). Based on in vitro verifications, Pedersen et al. (2003) suggested that mutant SCAD protein was prone to misfolding and thus to degradation and/or abnormal accumulation. It is also known that misfolded proteins may trigger cellular toxicity (Gregersen et al. 2008; Pedersen et al. 2008) although the molecular mechanism by which this occurs is not well understood. Interestingly, Margineantu et al. (2007) reported that the impairment of heat shock protein (hsp) 90, a molecular chaperone of protein folding, may disturb the ubiquitin–proteasome system, leading to the accumulation of abnormal protein and thus perhaps to mitochondrial fragmentation. As SCAD proteins are folded by hsp 60 (Pedersen et al. 2003), we examined whether the accumulation of SCAD mutant proteins was associated with mitochondrial changes. Immunostaining showed that each of the SCAD proteins (WT, mutants, and variants) was localized to the mitochondria (Fig. 4a), as reported previously (Naito et al. 1989a). Consistent with the conclusions of Margineantu et al., the proportion of cells with fragmented mitochondria was highest in transfectants expressing the mutant SCAD. In addition, the appearance of the fragmented mitochondria correlated well with the decrease in enzymatic activity. To determine whether mitochondrial fragmentation was specific to cells expressing the SCAD mutant proteins, the same experiment was carried out in cells transfected with the WT and K329E mutant MCAD, the most common mutation among patients with MCAD deficiency, and the transfectants were examined by immunostaining

(Sup. Fig. 2). No obvious differences in the mitochondria of WT cells and those expressing the K329E mutation were observed, suggesting that the SCAD mutants impose cellular alterations that are distinct from those due to mutations in the MCAD protein. A previous report suggested that mitochondrial fragmentation impairs mitochondrial homeostasis, and that the degree of mitochondrial damage correlated with the extent of mitochondrial fragmentation (Kim et al. 2007). A close relationship between mitochondrial fragmentation and neuronal degeneration, as well as several diseases, has also been described. For example, in Parkinson disease (PD), more extensive mitochondrial fragmentation is seen in cells exhibiting the PD-causing mutations (Dagda et al. 2009; Itoh et al. 2008; Knott et al. 2008; Lutz et al. 2009; Rodriguez-Hernandez et al. 2009). Therefore, in SCADD, mitochondrial fragmentation may reflect the mitochondrial damage induced by mutant SCAD proteins and may be related to the neuronal symptoms observed in these patients. Recently, pharmacological chaperone therapies against several lysosomal storage diseases by improving folding of mutated enzymes and their stabilities are proposed for future research (Parenti 2009). The same therapies might have the possibility for improving the clinical presentations of SCADD.

Finally, we investigated whether the mitochondrial fragmentation induced by mutated *ACADS* genes results in apoptotic cell death. As obvious differences in apoptotic activities between WT and the G108D mutants were not detected (Sup. Fig. 3), we investigated cellular autophagic activities. Immunoblot experiments showed high-level expression of LC3-II in G108D-expressing cells in which the severest mitochondrial fragmentation was observed. LC3-II is induced during autophagosome formation, and is therefore used as a molecular marker of autophagy, an important mechanism in the maintenance of protein homeostasis. The induction of autophagy has been described in several neuronal and muscle disorders (Bredesen 2008; Malicdan et al. 2008) and in neurodegeneration or neuronal cell death (Cheung et al. 2007; Gorman 2008; Knott et al. 2008). Thus, the induction of LC3-II in cells expressing SCAD mutations suggests a relationship between SCADD and the development of neuronal symptoms.

An association between *Acads* mutations and neurological findings was previously investigated in a mouse model (Tafti et al. 2003). BALB/cByJ mice carrying the G94D mutation in *Acads* showed slow theta oscillations, which may be related to a deterioration of cerebral cortex function. Tafti et al. suggested that a deficiency in the fatty acid metabolism pathway affects theta oscillations. These observations imply a relationship between neuronal disturbances and SCADD in the mouse. In our overexpression experiment using mutant SCAD, the induction of cellular autophagy was observed. So, it is interesting whether asymptomatic subjects have subclinical neurological damage. We think it significant to argue with this possibility. To clarify this point, further investigations including the existence of neurological signs in otherwise asymptomatic subjects are needed, and this might provide an important clue for further clarifying the pathophysiological and clinical features of patients with SCADD.

In this study, we found two female subjects who, as a result of MS/MS newborn screening, were suspected of having SCADD. Both subjects had compound heterozygous mutations, including a novel G108D mutation, in the *ACADS* gene. cDNAs prepared from the peripheral blood of these subjects were used to investigate the activity and solubility of the SCAD enzyme as well as the effects of the mutations on the mitochondria and on cellular autophagy. The expression of mutant SCAD, especially G108D, in transfected cells resulted in a severe decrease in SCAD enzymatic activity, a change in the enzyme's solubility, and the induction of both mitochondrial fragmentation and autophagy. However, as our results were derived from transient gene expression experiments, they cannot be extrapolated to the physiological nature of mutant SCAD proteins in vivo. Further investigations are needed to clarify the relationship between cellular autophagy and neurological symptoms and to determine the implications of our findings with respect to the development of clinical manifestations in patients with SCADD.

Acknowledgments This work was supported by a Grant-in-Aid for Young Scientist (B) No. 20790731 from Japan Society for the Promotion of Science and a grant from the Ministry of Health, Labor, and Welfare of Japan (Chief: Professor Seiji Yamaguchi). This work was carried out at the Analysis Center of Life Science, Hiroshima University.

Conflict of interest statement None declared.

References

Amendt BA, Greene C, Sweetman L, Cloherty J, Shih V, Moon A, Teel L, Rhead WJ (1987) Short-chain acyl-coenzyme A dehydrogenase deficiency. Clinical and biochemical studies in two patients. J Clin Invest 79:1303–1309

Bennett MJ, Gray RG, Isherwood DM, Murphy N, Pollitt RJ (1985) The diagnosis and biochemical investigation of a patient with a short chain fatty acid oxidation defect. J Inherit Metab Dis 8(Suppl 2):135–136

Bhala A, Willi SM, Rinaldo P, Bennett MJ, Schmidt-Sommerfeld E, Hale DE (1995) Clinical and biochemical characterization of short-chain acyl-coenzyme A dehydrogenase deficiency. J Pediatr 126:910–915

Bok LA, Vreken P, Wijburg FA, Wanders RJ, Gregersen N, Corydon MJ, Waterham HR, Duran M (2003) Short-chain Acyl-CoA dehydrogenase deficiency: studies in a large family adding to the complexity of the disorder. Pediatrics 112:1152–1155

Bredesen DE (2008) Programmed cell death mechanisms in neurological disease. Curr Mol Med 8:173–186

Cheung EC, McBride HM, Slack RS (2007) Mitochondrial dynamics in the regulation of neuronal cell death. Apoptosis 12:979–992

Coates PM, Hale DE, Finocchiaro G, Tanaka K, Winter SC (1988) Genetic deficiency of short-chain acyl-coenzyme A dehydrogenase in cultured fibroblasts from a patient with muscle carnitine deficiency and severe skeletal muscle weakness. J Clin Invest 81:171–175

Corydon MJ, Gregersen N, Lehnert W, Ribes A, Rinaldo P, Kmoch S, Christensen E, Kristensen TJ, Andresen BS, Bross P, Winter V, Martinez G, Neve S, Jensen TG, Bolund L, Kolvraa S (1996) Ethylmalonic aciduria is associated with an amino acid variant of short chain acyl-coenzyme A dehydrogenase. Pediatr Res 39:1059–1066

Corydon MJ, Andresen BS, Bross P, Kjeldsen M, Andreasen PH, Eiberg H, Kolvraa S, Gregersen N (1997) Structural organization of the human short-chain acyl-CoA dehydrogenase gene. Mamm Genome 8:922–926

Corydon MJ, Vockley J, Rinaldo P, Rhead WJ, Kjeldsen M, Winter V, Riggs C, Babovic-Vuksanovic D, Smeitink J, De Jong J, Levy H, Sewell AC, Roe C, Matern D, Dasouki M, Gregersen N (2001) Role of common gene variations in the molecular pathogenesis of short-chain acyl-CoA dehydrogenase deficiency. Pediatr Res 49:18–23

Dagda RK, Cherra SJ 3rd, Kulich SM, Tandon A, Park D, Chu CT (2009) Loss of PINK1 function promotes mitophagy through effects on oxidative stress and mitochondrial fission. J Biol Chem 284:13843–13855

Gorman AM (2008) Neuronal cell death in neurodegenerative diseases: recurring themes around protein handling. J Cell Mol Med 12:2263–2280

Gregersen N, Winter VS, Corydon MJ, Corydon TJ, Rinaldo P, Ribes A, Martinez G, Bennett MJ, Vianey-Saban C, Bhala A, Hale DE, Lehnert W, Kmoch S, Roig M, Riudor E, Eiberg H, Andresen BS, Bross P, Bolund LA, Kolvraa S (1998) Identification of four new mutations in the short-chain acyl-CoA dehydrogenase (SCAD) gene in two patients: one of the variant alleles, 511C→T, is present at an unexpectedly high frequency in the general population, as was the case for 625G→A, together conferring susceptibility to ethylmalonic aciduria. Hum Mol Genet 7:619–627

Gregersen N, Andresen BS, Corydon MJ, Corydon TJ, Olsen RK, Bolund L, Bross P (2001) Mutation analysis in mitochondrial fatty acid oxidation defects: Exemplified by acyl-CoA dehydrogenase deficiencies, with special focus on genotype-phenotype relationship. Hum Mutat 18:169–189

Gregersen N, Andresen BS, Pedersen CB, Olsen RK, Corydon TJ, Bross P (2008) Mitochondrial fatty acid oxidation defects—remaining challenges. J Inherit Metab Dis 31:643–657

Itoh T, Ito Y, Ohguchi K, Ohyama M, Iinuma M, Otsuki Y, Nozawa Y, Akao Y (2008) Eupalinin A isolated from *Eupatorium chinense* L. induces autophagocytosis in human leukemia HL60 cells. Bioorg Med Chem 16:721–731

Kang HT, Hwang ES (2009) Nicotinamide enhances mitochondria quality through autophagy activation in human cells. Aging Cell 8:426–438

Kim I, Rodriguez-Enriquez S, Lemasters JJ (2007) Selective degradation of mitochondria by mitophagy. Arch Biochem Biophys 462:245–253

Knott AB, Perkins G, Schwarzenbacher R, Bossy-Wetzel E (2008) Mitochondrial fragmentation in neurodegeneration. Nat Rev Neurosci 9:505–518

Lutz AK, Exner N, Fett ME, Schlehe JS, Kloos K, Lammermann K, Brunner B, Kurz-Drexler A, Vogel F, Reichert AS, Bouman L, Vogt-Weisenhorn D, Wurst W, Tatzelt J, Haass C, Winklhofer KF (2009) Loss of parkin or PINK1 function increases Drp1-dependent mitochondrial fragmentation. J Biol Chem 284:22938–22951

Malicdan MC, Noguchi S, Nonaka I, Saftig P, Nishino I (2008) Lysosomal myopathies: an excessive build-up in autophagosomes is too much to handle. Neuromuscul Disord 18:521–529

Malolepsza EB (2008) Modeling of protein misfolding in disease. Methods Mol Biol 443:297–330

Margineantu DH, Emerson CB, Diaz D, Hockenbery DM (2007) Hsp90 inhibition decreases mitochondrial protein turnover. PLoS One 2:e1066

Naito E, Indo Y, Tanaka K (1989a) Short chain acyl-coenzyme A dehydrogenase (SCAD) deficiency. Immunochemical demonstration of molecular heterogeneity due to variant SCAD with differing stability. J Clin Invest 84:1671–1674

Naito E, Ozasa H, Ikeda Y, Tanaka K (1989b) Molecular cloning and nucleotide sequence of complementary DNAs encoding human short chain acyl-coenzyme A dehydrogenase and the study of the molecular basis of human short chain acyl-coenzyme A dehydrogenase deficiency. J Clin Invest 83:1605–1613

Okada S, Ishikawa N, Shirao K, Kawaguchi H, Tsumura M, Ohno Y, Yasunaga S, Ohtsubo M, Takihara Y, Kobayashi M (2007) The novel IFNGR1 mutation 774del4 produces a truncated form of interferon-gamma receptor 1 and has a dominant-negative effect on interferon-gamma signal transduction. J Med Genet 44:485–491

Parenti G (2009) Treating lysosomal storage diseases with pharmacological chaperones: from concept to clinics. EMBO Mol Med 1:268–279

Pedersen CB, Bross P, Winter VS, Corydon TJ, Bolund L, Bartlett K, Vockley J, Gregersen N (2003) Misfolding, degradation, and aggregation of variant proteins. The molecular pathogenesis of short chain acyl-CoA dehydrogenase (SCAD) deficiency. J Biol Chem 278:47449–47458

Pedersen CB, Kolvraa S, Kolvraa A, Stenbroen V, Kjeldsen M, Ensenauer R, Tein I, Matern D, Rinaldo P, Vianey-Saban C, Ribes A, Lehnert W, Christensen E, Corydon TJ, Andresen BS, Vang S, Bolund L, Vockley J, Bross P, Gregersen N (2008) The ACADS gene variation spectrum in 114 patients with short-chain acyl-CoA dehydrogenase (SCAD) deficiency is dominated by missense variations leading to protein misfolding at the cellular level. Hum Genet 124(1):43–56

Peng TI, Jou MJ (2004) Mitochondrial swelling and generation of reactive oxygen species induced by photoirradiation are heterogeneously distributed. Ann N Y Acad Sci 1011:112–122

Rodriguez-Hernandez A, Cordero MD, Salviati L, Artuch R, Pineda M, Briones P, Gomez Izquierdo L, Cotan D, Navas P, Sanchez-Alcazar JA (2009) Coenzyme Q deficiency triggers mitochondria degradation by mitophagy. Autophagy 5:19–32

Tafti M, Petit B, Chollet D, Neidhart E, de Bilbao F, Kiss JZ, Wood PA, Franken P (2003) Deficiency in short-chain fatty acid beta-oxidation affects theta oscillations during sleep. Nat Genet 34:320–325

Taguchi N, Ishihara N, Jofuku A, Oka T, Mihara K (2007) Mitotic phosphorylation of dynamin-related GTPase Drp1 participates in mitochondrial fission. J Biol Chem 282:11521–11529

Tajima G, Sakura N, Yofune H, Nishimura Y, Ono H, Hasegawa Y, Hata I, Kimura M, Yamaguchi S, Shigematsu Y, Kobayashi M (2005) Enzymatic diagnosis of medium-chain acyl-CoA dehydrogenase deficiency by detecting 2-octenoyl-CoA production using high-performance liquid chromatography: a practical confirmatory test for tandem mass spectrometry newborn screening in Japan. J Chromatogr B Analyt Technol Biomed Life Sci 823:122–130

Tein I, Elpeleg O, Ben-Zeev B, Korman SH, Lossos A, Lev D, Lerman-Sagie T, Leshinsky-Silver E, Vockley J, Berry GT, Lamhonwah AM, Matern D, Roe CR, Gregersen N (2008) Short-chain acyl-CoA dehydrogenase gene mutation (c.319C>T) presents with clinical heterogeneity and is candidate founder

mutation in individuals of Ashkenazi Jewish origin. Mol Genet Metab 93:179–189

van Maldegem BT, Duran M, Wanders RJ, Niezen-Koning KE, Hogeveen M, Ijlst L, Waterham HR, Wijburg FA (2006) Clinical, biochemical, and genetic heterogeneity in short-chain acyl-coenzyme A dehydrogenase deficiency. JAMA 296:943–952

Wanders RJ, Vreken P, den Boer ME, Wijburg FA, van Gennip AH, IJlst L (1999) Disorders of mitochondrial fatty acyl-CoA beta-oxidation. J Inherit Metab Dis 22:442–487

European Journal of Medical Genetics 53 (2010) 383–388

Contents lists available at ScienceDirect

European Journal of Medical Genetics

journal homepage: http://www.elsevier.com/locate/ejmg

Original article

Determination of the deletion breakpoints in two patients with contiguous gene syndrome encompassing *CYBB* gene

Masafumi Yamada [a,*], Takashi Arai [b], Tsutomu Oishi [b], Norikazu Hatano [a], Ichiro Kobayashi [c], Mitsuru Kubota [d], Nobuhiro Suzuki [e], Minami Yoda [f], Nobuaki Kawamura [a], Tadashi Ariga [a]

[a] *Department of Pediatrics, Hokkaido University Graduate School of Medicine, North 15 West 7, Kita-ku Sapporo 060-8638, Japan*
[b] *Division of Infectious Disease, Saitama Children's Medical Center, Japan*
[c] *Department of Pediatrics, Kitami Red Cross Hospital, Japan*
[d] *Department of Pediatrics, Teine Keijinkai Hospital, Japan*
[e] *Department of Pediatrics, Sapporo Medical University School of Medicine, Japan*
[f] *Department of Pediatrics, Hakodate Municipal Hospital, Japan*

ARTICLE INFO

Article history:
Received 15 January 2010
Accepted 23 August 2010
Available online 21 September 2010

Keywords:
Deletion breakpoints
Contiguous gene syndrome
CGD
CYBB
Array CGH analysis
LCR(s)

ABSTRACT

X-linked chronic granulomatous disease is a primary immunodeficiency caused by mutations in *CYBB*. Although large deletions involving *CYBB* are known to cause contiguous gene syndrome (CGS), only a few patients have been studied precisely at the molecular levels. Our study determined the deletion breakpoints in two patients with CGS involving *CYBB* by array comparative genomic hybridization and the following PCR and DNA walking studies. The deletion size was 3.5 Mb in Patient 1 and 0.8 Mb in Patient 2. There were no homologous architectural features between the telomeric and centromeric breakpoint junctions in the deletions of either patient. However, the telomeric breakpoint of Patient 2 was embedded in a stretch of low-copy repeats and the centromeric breakpoint was also embedded in a stretch of short segments with significant sequence homology. These findings suggest the potential involvement of genome architecture in stimulating genomic rearrangements in Patient 2.

1. Introduction

Chronic granulomatous disease (CGD) is a primary immunodeficiency disease characterized by the inability of phagocytes to kill microorganisms because of a defect in the generation of reactive oxygen species. X-linked CGD (X-CGD) is the most common form of CGD. It is caused by mutations in the X-chromosome gene, *CYBB*, encoding gp91^{phox}. While the majority of patients have mutations within this gene, large deletions are known to cause contiguous gene syndromes (CGS), in which McLeod syndrome, ornithine transcarbamylase (OTC) deficiency, retinitis pigmentosa and/or Duchenne muscular dystrophy (DMD) accompany X-CGD [3,4,10,11]. Although intragenic deletions and duplications of the *DMD* gene have been extensively analyzed in a large group study [5], only a few CGS patients with lesions of this region have had their deletion breakpoints determined at the molecular level [3,11].

Array comparative genomic hybridization (CGH) is a powerful technique that is able to detect variations in DNA copy between a patient and normal sample over a wide region of the genome. This allows the identification of chromosomal regions in the patient's DNA which contain sequence gains and losses. Array CGH can be used to discover and evaluate the genomic rearrangements that may be present in the DNA of a patient with CGS.

In this study, we report on two patients with CGS involving *CYBB* whose deletion breakpoints were determined by array CGH and subsequent PCR and DNA walking analyses. Repetitive sequences near the breakpoints of the deletion seen in Patient 2 may have contributed to this rearrangement. The accurate description of deletion breakpoints in patients with CGS could lead to better

Abbreviations: X-CGD, X-linked chronic granulomatous disease; CGS, contiguous gene syndrome; CGH, comparative genomic hybridization; LCR(s), low-copy repeat(s); DMD, Duchenne muscular dystrophy; *DMD*, DMD gene; *FAM47A, B,* and *C*, Family with sequence similarity 47, member A, B, and C; *TMEM47*, transmembrane protein 47; *MAGEB16*, melanoma antigen family B, 16; CXorf, chromosome X open reading frame; *PRRG1*, proline-rich Gla (G-carboxyglutamic acid) 1; *FTHL19*, ferritin, heavy polypeptide-like 19; *LANCL3*, LanC lantibiotic synthetase component C-like 3; *XK*, X-linked Kx blood group gene; *CYBB*, cytochrome b-245 beta polypeptide; *DYNLT3*, dynein, light chain, Tctex-type 3; *SC4MOP*, sterol-C4-methyl oxidase pseudogene; *SYTL5*, synaptotagmin-like 5; *SRPX*, sushi-repeat-containing protein, X-linked; *RPGR*, retinitis pigmentosa GTPase regulator; *OTC*, ornithine transcarbamylase; *TSPAN7*, tetraspanin 7; *MID1IP1*, MID1 interacting G12-like protein; *BCOR*, BCL-6 interacting corepressor; *ATP6AP2*, ATPase, H+ transporting, lysosomal accessory; *MED14*, mediator complex subunit 14.

* Corresponding author. Tel.: +81 11 706 5954; fax: +81 11 706 7898.
E-mail address: yamadam@med.hokudai.ac.jp (M. Yamada).

1769-7212/$ – see front matter © 2010 Elsevier Masson SAS. All rights reserved.
doi:10.1016/j.ejmg.2010.08.003

understanding of deletion mechanisms and improve clinical characterization of these disorders.

2. Materials and methods

2.1. Patients

Patient 1 was an 8-year-old male. He was the first child born to non-consanguineous Japanese parents. At 36 h after birth, he presented with a generalized seizure resulting in cardiac arrest. Blood ammonia was found to be high (1,054 μg/dl). Elevated levels of urine orotic acid and markedly reduced OTC activity (0.46% of normal) in a liver biopsy specimen led to the diagnosis of OTC deficiency. Recurrent perianal abscesses and lymphadenitis from infancy, and pelvic abscess at the age of 3 years led to the diagnosis of CGD. This was confirmed by deficient respiratory burst (ROB) activity and decreased $gp91^{phox}$ expression in granulocytes by flow cytometry. These flow cytometric analyses were performed as described elsewhere [16]. Acanthocytosis was also revealed. So far no signs of retinitis pigmentosa had been detected. No exons of the *XK*, *CYBB* or *OTC* genes were amplified by PCR of genomic DNA. His mother had a single ROB-positive population in granulocytes, indicating she is a non-carrier for X-CGD.

Patient 2 was a 20-year-old male. He was the third child born to non-consanguineous Japanese parents. The second male child died from Pseudomonas aeruginosa septicemia of unknown etiology. This patient was diagnosed as having CGD by NBT test after recurrent perianal abscesses and pneumonia. Flow cytometric analysis demonstrated deficient ROB activity and $gp91^{phox}$ expression in granulocytes. No exons of the *XK* or *CYBB* genes were amplified by PCR of genomic DNA. His mother showed ROB-positive and ROB-negative populations in granulocytes, indicating she is a carrier for X-CGD. He received successful hematopoietic stem cell transplantation at the age of 20 years [13].

2.2. DNA isolation

Informed consent for genetic analysis was obtained from the two patients and their mothers under a protocol approved by Institutional Review Board of Hokkaido University Hospital. Genomic DNA was extracted from heparinized blood using SepaGene (Sankojunyaku, Tokyo, Japan).

2.3. Array CGH analysis

Array CGH analysis was performed with the Agilent kit (Agilent Technologies, Palo Alto, CA) as described elsewhere [5] with minor modifications. This kit uses a 60-mer oligonucleotide-based microarray to perform a genome-wide survey for copy variations, and allows molecular profiling of any detected genomic aberrations. One μg of DNA from a patient and a male control was double-digested with RsaI and AluI for 4 h at 37 degrees C. After column purification, each digested sample was labeled by random priming (Agilent Genomic DNA Labeling Kit) for 2 h using Cy3-dUTP for the patient DNA and Cy5-dUTP for the control DNA. Labeled products were purified by Microcon YM-30 filter units (Millipore, Billerica, MA). After probe denaturation and pre-annealing with Cot-1 DNA (Invitrogen, Carlsbad, CA), hybridization was performed at 65 degrees C

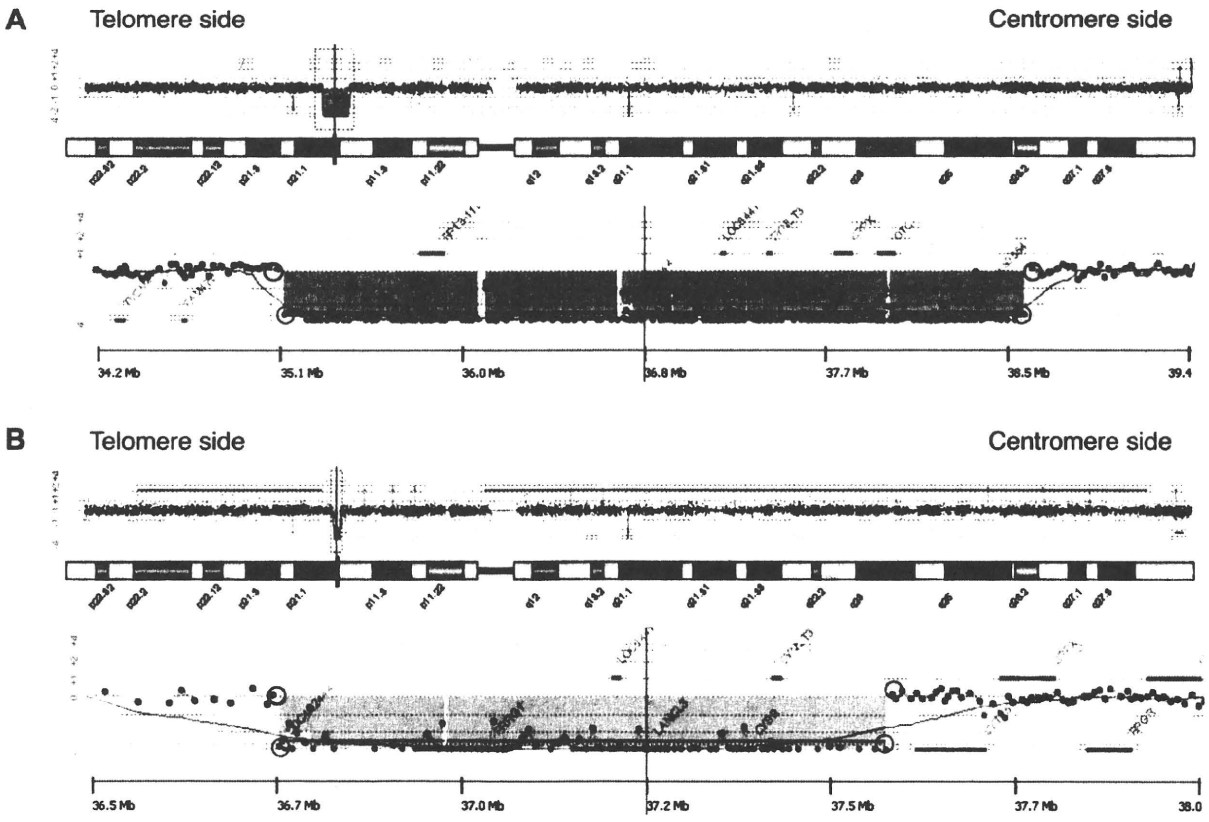

Fig. 1. The results of array CGH analysis in Patient 1 (A) and in Patient 2 (B). Blue and green belts indicated regions of continuously reduced copy number around Xp21.1 in Patient 1 and Patient 2, respectively. Red/blue empty circles on each end of the deletion represent detected/undetected array CGH probes.

Table 1
The UCSC genome positions and sequences of the detected/undetected array CGH probes.

Patient 1	
Telomere side, detected probe: chrX:035155777-035155836	AAATTTGATTTTGAACCTTTTCCTTGTGACCAATTGTGTAAGCCAACAAATACCTCTCTG
Telomere side, undetected probe: chrX:035181811-035181870	ACTAGGAATGATCAAACAATAAGAGAGACAATCCTTCTCTAAAACATCCTGACTCTCACC
Centromere side, undetected probe: chrX:038650675-038650734	GATTGCTAAATGGTTCTTCTTCATTTCCACTTATTCCAGTTTCATTTTAGCCACTTTGCC
Centromere side, detected probe: chrX:038683348-038683407	TTTCAGTGTTGGTCTTGCTATAAAACATTCTCTTTGGATGAACTATGATTGCCTTTGCTC
Patient 2	
Telomere side, detected probe: chrX:036769933-036769992	TGCCAAAGAATATATGCAGTGGAATATCTATTCCACTTTATGGGGCATAAAGATGAAGGA
Telomere side, undetected probe: chrX:036778864-036778923	GGAATCACGATATTCTATGCAAAACCAGAAGTCTACTTTATTTTTTCCCAGAGACACTGA
Centromere side, undetected probe: chrX:037606312-037606370	GTCAGAGAAAAAGAACTGTAAGAACTCGTCTACAAATAACAACCAGACTCAAGACCCTT
Centromere side, detected probe: chrX:037615536-037615595	TCTTGACAACACTCTCACTTAACAACTCACTCTCGAGAACTTTCACTTGTGTTTTATTTG

with rotation for 40 h. The hybridized array was analyzed with the Agilent scanner and the Feature Extraction software (v9.5.3.1). A graphical overview was obtained using the CGH analytics software (v3.5.14). The UCSC Genome Browser (May 2004) was used to retrieve the reference genome sequence (www.genome.ucsc.edu).

2.4. Determination of the deletion breakpoints by PCR-based studies

After identification of a deleted region by array CGH analysis in each patient, the telomeric and centromeric breakpoints of the deletions were determined by a 3-step PCR method, using AmpliTaq Gold (Applied Biosystems, Branchburg, NJ) as illustrated in Fig. 2. The 1st step was to confirm the presence or absence of adjacent sequences at each end of the deletions that had been detected or undetected in each patient using the array CGH analysis. PCR primers were prepared that corresponded to the two array CGH probes that flanked each end of the deletion. On the telomeric end of the deletion, these primers were named T1R (should be present in the patient) or T2F (should be absent in the patient) (Fig. 2). Corresponding nearby primers T1F and T2R were prepared, and PCR performed using the primer pairs T1F-T1R, and T2R-T2F. In the same way, PCR primers were prepared for the centromeric end of each deletion, named C1F, C1R, C2F and C2R (Fig. 2), and PCR performed. The 2nd step was to study the presence or absence of sequences between the CGH probes, using PCR with the T3F-T3R and C3F-C3R primer pairs, respectively. Based on this result, PCR study with subsequent primers on telomeric end (T4F-T4R, T5F-T5R, etc.) and centromeric end (C4F-C4R, C5F-C5R, etc.) was performed to further narrow down the deletion breakpoints on each end. Note that the primer names have been modified by addition of P1 or P2 in Fig. 3 to show which patient is being studied. The 3rd step was to amplify and sequence a PCR product that spanned the chromosome deletion recombination joint. For this, a telomeric forward (BPF) and centromeric reverse (BPR) primer pair were prepared, based on the prior analysis of the sequences present or absent in each patient's DNA (Fig. 2). All of the primer sequences will be shown upon request.

2.5. DNA walking analysis

A DNA walking analysis was subsequently performed to determine the deletion breakpoints in Patient 2, because PCR studies were unable to determine the breakpoints, as shown in Results. The regions around the centromeric deletion breakpoint were studied using the GenomeWalker Universal Kit (Clontech, Mountain View, CA) following the manufacturer's instructions. Briefly, after digestion with restriction enzymes (DraI, EcoRV, PvuII and StuI), genomic DNA from Patient 2 was ligated to GenomeWalker Adaptors. Then, gene-specific primary (5′-TGATTTGATCAGCTGAAGGAGACTTCC-3′) and nested (5′-CCTGTAGATGCTGGAGAGAGGACCAG-3′) primers, designed from sequences close to the centromeric breakpoint region, were used for PCR amplification in combination with the primary and nested primers for the GenomeWalker Adaptors. The resulting PCR products were sequenced following TOPO-TA cloning (Invitrogen). To confirm these results, gene-specific primers were designed to span the deletion breakpoints and PCR products were amplified from genomic DNA. Subsequent direct sequence analysis of the PCR products was performed.

3. Results

Array CGH analysis of genomic DNA from both patients delineated regions of continuously reduced copy number around Xp21.1, indicating large deletions (Fig. 1). Both patients had no significant copy number alterations in other parts of the whole genome. The deletion size was 3.5 Mb encompassing *XK* (X-linked Kx blood group gene), *CYBB*, *RPGR* (retinitis pigmentosa GTPase regulator) and *OTC* genes in Patient 1, and 0.8 Mb encompassing *XK* and *CYBB* genes in Patient 2. The genome positions and sequences of the adjacent detected/undetected array CGH probes on each end of the deletion are shown in Table 1. After confirming the presence/absence of the detected/undetected probe targets, we narrowed down the deletion breakpoints using 6 primer pairs on each end as described in Materials and methods (Figs. 2 and 3 and data not shown). In Patient 1, the 3rd step PCR amplified products spanning the deletion breakpoints (Fig. 4A). Direct sequence analysis of the PCR products demonstrated that the deletion breakpoints were chrX:35,168,892 and chrX:38,655,273 with the deletion length of 3,486,381 bp (Fig. 5A). The telomeric breakpoint was intergenic between the loci *FAM47B* (Family with sequence similarity 47, member B) and *MAGEB16* (Melanoma antigen family B, 16) (Fig. 4C). The centromeric breakpoint was intergenic between the loci *MID1IP1* (MID1 interacting protein 1) and *BCOR* (BCL-6 interacting corepressor isoform 1). The known disease-causing genes involved in the deletion were *XK*, *CYBB*, *RPGR*, *OTC* and *TSPAN7* (tetraspanin 7).

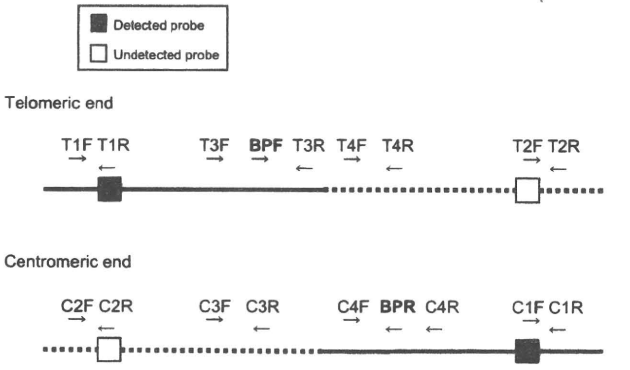

Fig. 2. Schematic representation of PCR-based determination of the deletion breakpoints. The filled (■) and empty (□) boxes represent detected and undetected probes used in array CGH analysis, respectively. The horizontal solid/dotted lines indicate the present/absent genomic regions.

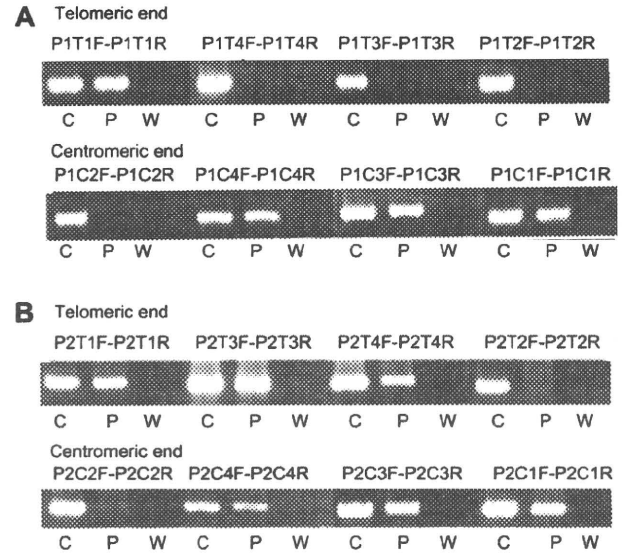

Fig. 3. The results of the 1st and 2nd steps of PCR-based studies in Patient 1 (A) and in Patient 2 (B) C: A normal control, P: Patient, W: Water.

On the other hand, the deletion breakpoints of Patient 2 could not be determined by the PCR-based method, because the 3rd step PCR did not amplify any products after narrowing down the deletion breakpoints. UCSC Blat and NCBI BLAST (http://blast.ncbi.nlm.nih.gov/Blast.cgi) search revealed the regions around the telomeric breakpoint shared highly homologous sequences with those of chromosome 6 and 13, which might be associated with the failure to narrow down the telomeric breakpoint. In fact, PCR products amplified with P2T4F-P2T4R primers did not contain the sequence between the two primers (data not shown). Therefore, we next approached the breakpoints from the centromeric side. The sequence obtained from DNA walking analysis spanned the deletion breakpoints, and showed the telomeric and centromeric sequences connected each other. To confirm this result, gene-specific primers were designed to span the deletion breakpoints and PCR products were amplified from genomic DNA. Subsequent direct sequence analysis of the PCR products demonstrated the deletion breakpoints

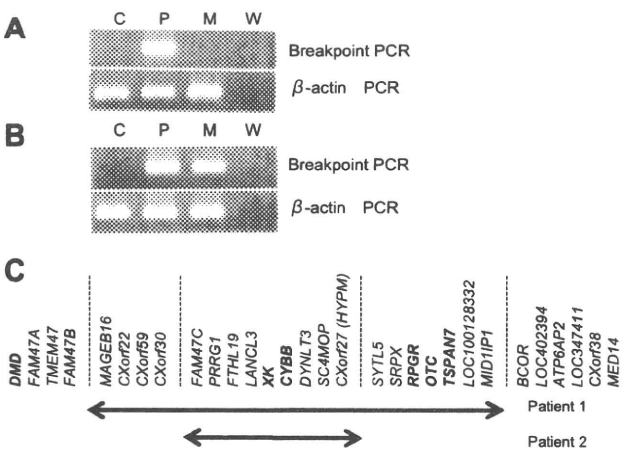

Fig. 4. The results of the PCR study spanning the deletion breakpoints (Breakpoint PCR) in Patient 1 (A) and in Patient 2 (B) C: A normal control, P: Patient, M: Mother, W: Water C: The genes involved in the deletions are shown by arrows. Known disease-causing genes were indicated by bold letters.

as chrX:36,775,400 and chrX:37,610,734 with a deletion length of 835,334 bp. There was a 36-bp insertion between the breakpoints (Figs. 4B and 5B). The sequence of this 36-bp insertion completely matched a forward sequence located about 8 kb upstream of the telomeric breakpoint (chrX:36,767,280 -chrX:36,767,315) (Fig. 6). This upstream sequence was confirmed to be present at its original position in the patient's DNA (data not shown). And interestingly, this 36-bp sequence also matched a reverse sequence located about 400 kb downstream of the telomeric breakpoint (chrX:37,183,818 - chrX:37,183853), which was in the middle of the deletion (Fig. 6). The telomeric and centromeric breakpoints were both intergenic between the loci *CXorf30* (chromosome X open reading frame 30) and *FAM47C*, and between *CXorf27* and *SYTL5* (Synaptotagmin-like 5), respectively (Fig. 4C). The known disease-causing genes involved in the deletion were *XK* and *CYBB*.

The breakpoint PCR did not amplify the products in Patient 1's mother but did in Patient 2's mother (Fig. 4). Direct sequence analysis of the breakpoint PCR products amplified in Patient 2's mother demonstrated exactly the same sequence as was seen in Patient 2. These results indicated that a *de novo* deletion occurred in Patient 1, whereas the deletion was inherited from his mother in Patient 2. These results are consistent with the tests of ROB activity.

4. Discussion

In this study, we analyzed two patients with CGS encompassing *CYBB* and determined their deletion breakpoints by array CGH followed by PCR and DNA walking studies.

So far, several patients with Xp11.4-Xp21.1 deletions have been reported and summarized [4]. Deardorff et al. classified these deletions into 4 categories: (a) deletions of approximately 10 Mb including more than DMD through OTC, (b) deletions of >5 Mb from DMD telomeric to OTC, (c) deletions <5 Mb centromeric of DMD including OTC, and (d) deletions of <5 Mb from centromeric of DMD to telomeric of OTC. There have been no recurrent genomic rearrangements documented. According to the classification described by Deardorff et al., the deletions of Patient 1 and Patient 2 belong to (c) and (d), respectively. None of the reported deletions were the same in terms of the deletion length and breakpoints.

Both recurrent and non-recurrent genomic rearrangements have been observed in human genomic disorders. Non-allelic homologous recombination (NAHR) mediated by two low-copy repeats (LCRs) as recombination substrates has been elucidated to be one of the major mechanisms for recurrent genomic rearrangements. These are characterized by a common size and fixed breakpoints (that is, a breakpoints cluster) [6,8,12]. LCRs, also known as segmental duplications, are continuous portions of DNA that map to two or more genomic locations, and are characterized by a high degree of identity (commonly >95%) and length of more than 1 kb [6,8,12]. NAHR mediated by LCRs accounts for various genomic disorders including 22q11.2 deletion syndrome [2], Williams-Beuren syndrome [1], Sotos syndrome [14] and Charcot-Marie-Tooth disease type 1A [12].

On the other hand, non-recurrent genomic rearrangements are characterized by different sizes and distinct breakpoints. Hastings et al. [7,8], have reviewed the characteristics of this type of rearrangement. First, chromosomal structural changes can be complex: they can have short sequences from elsewhere inserted at the breakpoints. Second, most of the non-recurrent genomic rearrangements occur at sites of microhomology, which is a short segment (2–15 bp) of limited homology. Third, although the non-recurrent breakpoints do not coincide with LCRs, they tend to occur in the vicinity of regions that are rich in LCRs. Microhomology-mediated break-induced replication (MMBIR) is recently proposed to be the main mechanism of non-recurrent genomic rearrangements,